1   Meridional contrasts in productivity changes driven by the opening of

2   Drake Passage

3

4   Jean-Baptiste Ladant[1,2,3*], Yannick Donnadieu[1,4], Laurent Bopp[2,3], Caroline H.

5   Lear[5], Paul A. Wilson[6]

6

7   *Corresponding author. Email: jbladant@gmail.com

8   [1]Laboratoire des Sciences du Climat et de l'Environnement, LSCE-IPSL, CEA / CNRS /

9   UVSQ, Université Paris-Saclay, Gif-sur-Yvette, France.

10   [2]Ecole Normale Supérieure, Département de Géosciences, Paris, France.

11   [3]LMD / IPSL, CNRS / ENS / Ecole Polytechnique / UPMC, Paris, France.

12   [4]Aix Marseille Université, CNRS, IRD, Coll. France, CEREGE, Aix-en-Provence, France.

13   [5]School of Earth and Ocean Sciences, Cardiff University, Cardiff, UK.

14   [6]Ocean and Earth Science, National Oceanography Centre Southampton, University of

15   Southampton, Southampton, UK.

16

17   **Keypoints**

18   • Productivity changes following Drake Passage opening are explored using the IPSL model

19   and compared with data from the late Eocene and early Oligocene.

20   • Drake Passage opening drives a decrease in productivity in the low latitudes and spatially

21   heterogeneous patterns in the high latitudes.

22   • Agreement between proxy records and model results indicate that Drake Passage opening

23   has driven part of the late Eocene productivity changes.

24

Abstract

Changes in atmospheric pCO_2 are widely suggested to have played a major role in both the long-term deterioration of Cenozoic climate and many superimposed rapid climate perturbations such as the pivotal Eocene-Oligocene transition. Changes in marine productivity affecting the biological oceanic carbon pump represent one possible cause of past CO_2 variability. Here, we explore the relationship between ocean gateway change and marine biogeochemistry. Specifically, we use a fully coupled atmosphere-ocean-biogeochemical model (IPSL-CM5A) to examine global ocean paleoproductivity changes in response to the opening of Drake Passage. In our simulations, we find that Drake Passage opening yields a spatially uniform decrease in primary productivity in the low latitude oceans while the high latitude response is more spatially heterogeneous. Mechanistically, the low latitude productivity decrease is a consequence of a fundamental reorganization of ocean circulation when Drake Passage opens driven by the isolation of the Southern Ocean from low latitude water masses. Nutrient-depletion in the low latitudes is driven by a marked decrease in the intensity of deep convection in the Southern Ocean, which drives the accumulation of nutrients at depth and their depletion in the intermediate and upper ocean, especially away from sites of subduction. In the high latitudes, the onset of the Antarctic Circumpolar Current in the model exerts a strong control both on nutrient availability but also on regions of deep-water formation. The qualitative agreement between geographically diverse long-term paleoproductivity records and the simulated variations suggests that Drake Passage opening may contribute to the long-term paleoproductivity signal.

Introduction

Tectonic opening of Southern Ocean gateways constitutes one of the most fundamental changes in Cenozoic boundary conditions because of the capacity to alter global ocean circulation and climate [*Barker and Burrell*, 1977; *Kennett*, 1977]. In a seminal paper, *Kennett* [1977] proposed that the opening of these gateways (Drake and Tasman Passages) to deep circulation was instrumental in initiating sustained Antarctic glaciation. This sequence of events is suggested to have initiated during the late Eocene [*Matthews and Poore*, 1980; *Miller et al.*, 1991; *Lear et al.*, 2000; *Stickley et al.*, 2004; *Lagabrielle et al.*, 2009], although debate is ongoing about the timing of full gateway opening to a deep and wide current system [*Barker et al.*, 2007; *Katz et al.*, 2011; *Scher et al.*, 2015]. This appealing hypothesis suggests that the opening of Drake Passage (DP) and of the Tasman gateway would have engendered the onset of an Antarctic Circumpolar Current (ACC), thermally isolating the Antarctic continent from water masses sourced in the lower latitudes and permitting the growth of an extensive Antarctic ice sheet (AIS). However, this ocean gateway hypothesis has subsequently lost some ground because the results of numerical model experiments have been unable to robustly demonstrate that the sole climatic impact of DP (or Tasman gateway) opening was sufficient to initiate the glaciation [*Mikolajewicz et al.*, 1993; *DeConto and Pollard*, 2003; *Huber and Nof*, 2006; *Sijp et al.*, 2011; *Goldner et al.*, 2014]. Instead, modelling studies have pointed to a CO_2 decline as the primary driver of AIS initiation through atmospheric radiative cooling [*Mikolajewicz et al.*, 1993; *DeConto and Pollard*, 2003; *Huber et al.*, 2004]. The remarkable match between observations [*Coxall et al.*, 2005; *Coxall and Wilson*, 2011] and model predictions [*DeConto and Pollard*, 2003; *Ladant et al.*, 2014] of the structure of the deep sea oxygen isotope record across the Eocene-Oligocene transition (EOT) and paleo-CO_2 reconstructions for this interval [*Pearson et al.*, 2009; *Pagani et al.*, 2011; *Heureux and Rickaby*, 2015] lend support to the CO_2 hypothesis. Yet these CO_2

75 reconstructions are far from well-developed and the influence of ocean gateway opening and

76 CO_2 forcing need not be mutually exclusive [*Egan et al.*, 2013; *Lear and Lunt*, 2016;

77 *Elsworth et al.*, 2017].

78   There exists a rich literature documenting long-term changes in oceanic carbon

79 cycling associated with Cenozoic climate deterioration including across the pivotal EOT

80 thanks to scientific ocean drilling [e.g., *Siesser*, 1995; *Schumacher and Lazarus*, 2004; *Faul*

81 *and Delaney*, 2010; *Griffith et al.*, 2010; *Coxall and Wilson*, 2011; *Pälike et al.*, 2012; *Egan*

82 *et al.*, 2013; *Moore et al.*, 2014; *Plancq et al.*, 2014; *Villa et al.*, 2014]. Paleoproductivity

83 reconstructions from the data – taken here to mean export production of organic matter to the

84 deep ocean since most paleo data studies inherently quantify export production rather than

85 primary productivity – display spatially heterogeneous long-term variations between the late

86 Eocene and the Oligocene (Table 1). Data from the northern high-latitudes are lacking but

87 records from the southern high-latitudes generally document paleoproductivity increases from

88 the Eocene into the Oligocene [*Schumacher and Lazarus*, 2004; *Plancq et al.*, 2014; *Villa et*

89 *al.*, 2014] while the low latitudes record a general decrease [*Schumacher and Lazarus*, 2004;

90 *Griffith et al.*, 2010; *Moore et al.*, 2014].

91   Numerical modelling studies have investigated the role of DP opening on global ocean

92 circulation and climate with spatially resolved Earth system models [*Mikolajewicz et al.*,

93 1993; *Toggweiler and Bjornsson*, 2000; *Sijp and England*, 2004; *Sijp et al.*, 2009; *Zhang et*

94 *al.*, 2010; *Sijp et al.*, 2011; *Yang et al.*, 2014; *Fyke et al.*, 2015; *England et al.*, 2017]. In

95 contrast, modelling of ocean biogeochemical changes across the late Eocene and Oligocene

96 has been limited. Most work of this type has been undertaken using either numerical box

97 models focusing specifically on the Eocene-Oligocene Transition itself [*Zachos and Kump*,

98 2005; *Merico et al.*, 2008; *Armstrong McKay et al.*, 2016] or using the UVic earth system

99 model of intermediate complexity (EMIC) integrating a biogeochemical component [*Pagani*

100 *et al.*, 2011; *Fyke et al.*, 2015]. Box models are powerful tools to investigate the credibility of

101 competing hypotheses at the global scale but they cannot be used to confront localized

102 paleoproductivity reconstructions. On the other hand, results from experiments using the

103 UVic EMIC suggest that the successive opening of DP and of the Panama seaway through

104 Cenozoic time would have exerted a major influence on the inter-basin carbon reservoir and

105 in setting the modern dissolved inorganic carbon gradients between basins [*Fyke et al.*, 2015].

106 *Pagani et al.* [2011] utilize an Eocene UVic simulation to generate Eocene-Oligocene surface

107 ocean phosphate concentrations, which they further use to compute surface ocean CO_2

108 concentrations to ultimately constrain their reconstructions of atmospheric CO_2 across the

109 EOT. Their results also suggest that, compared to modern, the surface ocean phosphate

110 concentration increases in the low latitudes and decreases in the high latitudes.

111   Here, we revisit the question of the biogeochemical impacts of DP using a more

112 sophisticated, fully coupled, IPCC-class model with, for the first time, a focus on

113 paleoproductivity changes and we compare our results with long-term records of productivity

114 change from the late Eocene to Oligocene. It should be noted that *Winguth et al.* [2012] also

115 applied a fully-coupled IPCC-class GCM to investigate paleoproductivity changes during the

116 Eocene, but their focus was the PETM and as such they realized simulations at different CO_2

117 rather than with open or closed gateways. Assessing the role DP opening played in driving

118 paleoproductivity changes during the late Eocene and Oligocene is important because of its

119 influence on the global carbon cycle and in particular pCO_2 variations, via changes in the

120 oceanic biological pump (see *Hain et al.* [2014] for a review). In the following, we explore

121 the effects of opening DP on long-term productivity changes using a similar approach to that

122 of *Fyke et al.* [2015] and *Elsworth et al.* [2017] in that we employ continental and

123 bathymetric configurations altered from those of present-day. In this respect, strictly

124 speaking, our experiment is a paleogeography sensitivity simulation rather than a simulation

125 of Eocene-Oligocene events. Nevertheless, our approach allows us to isolate the effect of DP

126 opening on global climate and productivity and to make a semi-quantitative comparison to

127 proxy records. Here we focus on comparing our results to records spanning the late Eocene

128 and early Oligocene – the canonical interval for which DP opening is invoked as a climate

129 forcing mechanism – but the possibility that a fully developed ACC was only established

130 during the late Miocene [e.g., *Dalziel et al.*, 2013] also lends our results a longer-term

131 Cenozoic relevance.

132

133 **Models**

134   The results presented in this study are obtained with the IPSL-CM5A Earth System

135 Model [*Dufresne et al.*, 2013], which includes both a representation of the physical

136 atmosphere-ocean-land-sea ice interactions and of the global carbon cycle. Its configuration

137 combines the atmospheric model LMDz [*Hourdin et al.*, 2013], the land-surface model

138 ORCHIDEE [*Krinner et al.*, 2005] and the ocean model NEMOv3.2 [*Madec*, 2008]. The

139 OASIS coupler [*Valcke*, 2006] is used to interpolate and exchange variables and synchronize

140 the models [*Dufresne et al.*, 2013]. Only succinct details about the models will be given here

141 because their full description can be found in *Dufresne et al.* [2013] (see also *Kageyama et al.*

142 [2013] for a description of the model used in paleo configurations for the Last Glacial

143 Maximum and the mid-Holocene). LMDz solves the equation of atmospheric motion on a

144 regular longitude-latitude grid using σ-P vertical coordinates. The resolution used in this

145 study is 96x95x39 (lon. x lat. x vert.), corresponding to 3.75° of longitude and 1.875° of

146 latitude, and 39 vertical levels irregularly distributed. ORCHIDEE runs on the same grid as

147 LMDz and contains a land-surface scheme that simulates both the energy and water cycles of

148 soils and vegetation and a routing scheme that routes precipitated water to the ocean. 12 Plant

149 Functional Types (PFT) define the vegetation. Although the vegetation cover is imposed in

150 this version of IPSL-CM5A, the PFT phenology is computed interactively given the

151 atmospheric state simulated by LMDz. The NEMO model comprises an ocean dynamics

152 component (OPA, *Madec* [2008]), a thermodynamic-dynamic sea-ice model (LIM2, *Fichefet*

153 *and Morales Maqueda* [1997]), and an ocean biogeochemistry model (PISCES, *Aumont and*

154 *Bopp* [2006]). NEMO uses a tripolar grid in order to avoid North Pole singularity [*Madec and*

155 *Imbard*, 1996], for both dynamics and physics. It has a nominal latitudinal resolution of 2°,

156 increasing up to 0.5° at the Equator, and a longitudinal resolution of approximately 2° and 31

157 unequally spaced vertical levels, the thickness of which varies from 10 m near the surface to

158 500 m at the bottom. PISCES includes a simple representation of the marine ecosystem and of

159 the main oceanic biogeochemical cycles [*Aumont and Bopp*, 2006]. It explicitly represents

160 two classes of phytoplankton (nanophytoplankton and diatoms), two classes of zooplankton,

161 five pools of nutrients (phosphate, nitrate, silicic acid, ammonium and iron), two classes of

162 particulate organic carbon (small and large) and semi-labile dissolved organic carbon. It also

163 includes dissolved and particulate inorganic carbon, alkalinity and dissolved oxygen. The

164 main biogeochemical interactions, such as photosynthesis, respiration, grazing, particle

165 aggregation and sinking, and remineralization, dictate the spatio-temporal evolution of each

166 pool with respect to each other. Phytoplankton growth is limited by the aforementioned

167 nutrients and by light availability. Ratios of C:N:P in the organic pools are kept constant

168 following *Takahashi et al.* [1985], whereas Fe:C ratios for both phytoplankton classes and

169 Si:C ratios for diatoms are prognostically simulated as a function of the external concentration

170 of nutrients and light availability [*Aumont and Bopp*, 2006]. The full description of the

171 version of PISCES used in this study can be found in *Aumont and Bopp* [2006]. All these

172 models have been validated and used, either separately or together within the IPSL-CM5A

173 model, over a variety of climates that include pre-Quaternary climates [e.g., *Contoux et al.*,

174 2015; *Tan et al.*, 2017], LGM [e.g., *Mariotti et al.*, 2012; *Kageyama et al.*, 2013],

175   preindustrial [*Le Mézo et al.*, 2017] and present-day and future climates [e.g., *Aumont and*

176   *Bopp*, 2006; *Bopp et al.*, 2013; *Tagliabue et al.*, 2014], including the latest IPCC exercise.

177   In a first step, two simulations are run with the fully coupled IPSL-CM5A model.

178   Both simulations have a preindustrial land-sea mask, from which the geometry of the Panama

179   Seaway has been altered to represent mid-Cenozoic tectonic configurations (in practice, this

180   means replacing continental grid points by oceanic grid points, see Supplementary Fig. 1). In

181   addition, the land-sea mask of the first simulation, named DC (for Drake Closed), has been

182   modified to add terrestrial points at the Drake Passage to simulate its closure. Conversely, the

183   Drake Passage is left unchanged from that of the preindustrial in the land-sea mask of the

184   second simulation, named DO (Drake Opened). Compared to preindustrial conditions, ice

185   sheets over polar continents have been removed and replaced by tundra-like vegetation but

186   otherwise the preindustrial vegetation cover is kept for both simulations. The ocean is

187   initialized as homogeneous in salinity (34.5 kg.m^{-3}) and with surface temperature following a

188   latitudinal profile ranging from 9°C at the poles to 36°C at the equator. The deep ocean is

189   initialized at a uniform temperature of 7°C (Supplementary Fig. 2). There is no sea ice at the

190   beginning of the simulations. We prescribe a CO_2 concentration of 1120 ppm, which is

191   consistent with most of the records of paleo-CO_2 levels for the Eocene [*Beerling and Royer*,

192   2011] and justifies the absence of ice sheets over the poles because the inception of ice over

193   Antarctica is thought to occur at lower CO_2 levels [*Gasson et al.*, 2014; *Ladant et al.*, 2014;

194   *Heureux and Rickaby*, 2015]. Each of the two experiments is run for 1000 years. We

195   acknowledge here that longer integrations (>= 3000 years) are desirable but we are precluded

196   by the computational performances of this version of the IPSL-CM5A model. However, after

197   1000 years, the surface ocean is in equilibrium and the very small residual trend (< 0.1

198   °C/century) that exists in the deep ocean is unlikely to significantly affect the outcomes of the

199   study.

200   Oceanic biogeochemical equilibrium typically requires longer simulations to be

201   attained than the dynamical equilibrium [*Séférian et al.*, 2016]. In a second step, we run

202   offline simulations of the PISCES model in order to be closer to the biogeochemical

203   equilibrium. PISCES is initialized with the oceanic biogeochemical outputs from the last year

204   of DC and DO coupled experiments and forced by the ocean dynamical fields of DC and DO.

205   In detail, the last 100 years of ocean dynamics outputs are passed to PISCES-offline in a

206   repetitive sequence (that is, after each 100 years of simulation, the ocean forcing is repeated

207   for the next 100 years). The simulations DC-P (for DC-PISCES) and DO-P are run for 2000

208   years to ensure equilibrium of the biogeochemical fields. One caveat must be noted here. In

209   this version of IPSL-CM5A, the nutrient delivery to the ocean is fixed. This is an important

210   simplification because under different climates the global amount of nutrients as well as the

211   spatial distribution of nutrient inputs to the ocean (i.e., the intensity and location of the river

212   flows) will be altered. However, as our purpose is to isolate the climatic and biogeochemical

213   effects of DP opening only and to provide insights into its long-term signature in the proxy

214   record, we have kept present-day nutrient inputs in the simulations.

215   In the following, we refer to the closed (open) Drake Passage simulations by DC (DO)

216   regardless of whether we consider the fully coupled IPSLCM5A or the PISCES-offline

217   simulation, but dynamical results utilize the IPSLCM5A simulations while the

218   biogeochemistry is discussed using the PISCES-offline simulations.

219

220   **Results**

221   In the simulations, the opening of DP significantly alters paleoproductivity (i.e., paleo

222   export production). Figure 1 shows the DC and DO global annual export production of

223   organic carbon at 100 m, a commonly used measure of the carbon export into the deep ocean.

224   The major areas contributing to this export are similar in the two simulations (Fig. 1) but in

225 regions such as the low latitude Indian and Pacific oceans, productivity uniformly decreases

226 with DP opening (Figs. 1 and 2). In contrast, in the Southern Ocean, while productivity

227 decreases in the Atlantic sector, it increases in the Pacific and Indian sectors when DP opens.

228 In the zonal average, opening DP yields an increase in carbon export to the deep ocean in the

229 southern high latitudes but a decrease in the low latitudes and northern high latitudes. This

230 dipole pattern of increase in the southern high latitudes and decrease in the low latitudes

231 agrees with the meridional contrast seen in the data (Table 1). The spatial pattern of

232 increase/decrease in our simulations also compares favourably with observations from various

233 drilling locations (Fig. 1).

234 The observed patterns of paleoproductivity change are the consequence of alterations

235 in ocean circulation, which controls the supply of nutrients, essentially nitrate and phosphate,

236 brought from the deep or sub-surface ocean to the surface. The zonally averaged

237 redistribution of nutrients follows a dipole pattern on the vertical (Fig. 3) with a decrease in

238 the intermediate and upper ocean and an increase at depth when DP opens, except in the

239 highest latitudes of the Southern Ocean (> 60°S). Indeed, in this region, an increase in the

240 concentration of nutrients occurs throughout the whole water column when DP opens.

241 Vertical gradients in the upper 500 m confirm the decreased nutrient availability in the low

242 latitudes of each basin in DO and the increase in the southern high latitudes (Fig. 4), except in

243 the upper 100 m of the Atlantic sector.

244 The redistribution of nutrients in our simulations directly follows the reorganization of

245 the oceanic thermohaline circulation (Figs. 5 and 6). In DC, the circulation is dominated by a

246 vigorous Southern Hemisphere overturning cell of up to 30 Sv (Fig. 5), which is fed via deep

247 convection (> 2000 m) in the Pacific and Atlantic sectors of the Southern Ocean (Fig. 6).

248 These deep waters then fill the deep ocean globally, circulate northward in the abyss, are

249 strongly upwelled in the low latitudes at depth and return southward between 500 m and 1500

250   m depth. There is no deep-water formation in the Northern Hemisphere and the closed DP

251   prevents the existence of a well-developed ACC. A wind-driven circumpolar circulation still

252   develops around Antarctica under the influence of the Westerlies (Supplementary Fig. 3),

253   which generates upwelling cells carrying waters from the southward branch of the overturning

254   circulation to the surface. Some of these waters then feed the abyssal circulation through deep

255   convection around Antarctica while the remaining fraction is advected northward to feed

256   intermediate and modal ocean circulation [*Toggweiler and Samuels*, 1993]. The absence of a

257   well-developed ACC leads to enhanced export of warm and salty subtropical waters into the

258   Southern Ocean, increasing the intensity of deep water formation there as well as the

259   southward ocean heat transport [*Sijp and England*, 2004].

260   Opening DP strongly modifies the global ocean circulation (Fig. 5). Arguably, the

261   major difference lies in the appearance of a vigorous modern-like ACC (Supplementary Fig.

262   3), which interconnects the three major basins from top to bottom and generates a relatively

263   deep Deacon Cell (~ 2000 m), which reflects the existence of deep upwelling cells. The latter

264   are deeper and more expanded towards Antarctica relative to DC, as shown by the overlain

265   isopycnals on Figs. 3a and 3b, and then feed the abyssal and the intermediate/modal

266   circulations as in DC. Abyssal waters formed around Antarctica remain however mostly

267   confined below 2000 m (Fig. 5). The existence of a well-developed ACC limits the advection

268   of warm and salty subtropical waters to the Southern Ocean, which reduces the intensity of

269   deep convection (Fig. 6) because at high latitudes, salinity exerts the dominant control over

270   the stratification of ocean waters [*Ferreira et al.*, 2010; *Yang et al.*, 2014]. A very weak

271   overturning cell appears in the Nordic Seas, promoting modest intermediate water formation

272   (up to ~ 700 m, Fig. 6). The rates of global overturning in DO are thus greatly reduced

273   relative to DC, increasing the residence time of water in the deep ocean.

274   The transition from a well-ventilated DC to a more stagnant DO ocean thereby drives

275   accumulation of nutrients at depth and depletion in the intermediate and upper ocean in DO

276   relative to DC because the reduced ventilation acts to 'de-homogenize' the ocean (Fig. 3c). In

277   DC, the much stronger abyssal low latitudes upwelling allow nutrients to be more rapidly

278   exported in the vigorous southward branch of the overturning circulation whereas in DO,

279   these nutrient-rich waters are confined below 2000 m, thus increasing the nutrient

280   concentrations below 2000 m and decreasing them above 2000 m in DO relative to DC.

281   In both simulations, nutrient-enriched waters are then carried to the surface by the

282   Southern Ocean upwelling cells (Figs. 3a and 3b) but because of the intensity and shape of the

283   overturning circulation, the upwelled waters contain more nutrients in DC relative to DO.

284   This is why the subsurface nutrient concentrations between 40°S and 60°S decrease in DO.

285   However, because the upwelling cells are deeper and expand slightly southward in DO, the

286   subsurface of the highest latitude oceans (> 60°S) is enriched in nutrients relative to DC (Figs.

287   3c and 4, again except for the upper 100 m in the Atlantic sector).

288   The decrease in subsurface nutrient concentration in the 40°S-60°S area in DO has

289   important consequences for the low latitude nutrient supply. Indeed, the intermediate and

290   modal waters (IMW) formed in this area are then advected to feed low latitude subsurface

291   waters [*Toggweiler and Samuels*, 1993; *Sarmiento et al.*, 2004]. Because the IMW are poorer

292   in nutrients when DP is open, the supply of nutrients to the low latitudes decreases. In

293   addition, the slight increase in the tilt of the isopycnals in DO between 40°S and 50°S

294   indicates that IMW sink deeper than in DC and consequently may contribute to the decrease

295   in nutrient supply to the subsurface low latitudes waters in DO.

296   While low latitude productivity and export changes are well explained by the

297   decreased nutrient availability resulting from the less dynamic DO ocean, additional processes

298   contribute to the modelled changes in productivity in the Southern Ocean. Indeed, convective

299   mixing, associated with deep-water formation in winter and wind-driven circumpolar

300   currents, heavily influences export productivity patterns at these latitudes (Figs. 1 and 6). In

301   the Pacific sector, the DO deep-water convective areas are significantly shallower and

302   narrower but remain deep enough to increase the productivity because the convection affects

303   water masses significantly enhanced in nutrients. Following the onset of the ACC, a large

304   convection zone appears in the southern Indian Ocean around 50°S, which, albeit relatively

305   shallow (up to 500 m), drives a large increase in productivity (Fig. 1). Similarly, the wider

306   convection zone just offshore Antarctica at the longitude of Africa generates productivity

307   increase. Finally, in the Atlantic sector, the opposite occurs. Deep-water convection is

308   completely shut down in DO in the central South Atlantic Ocean, leading to a substantial area

309   of decreased productivity.

310   Because the PISCES model allows the explicit representation of nanophytoplankton

311   and diatoms, we can also assess the role of these different groups in driving the modelled

312   primary productivity changes (Fig. 7 and Supplementary Fig. 4). In the low latitudes, the

313   decrease in primary productivity is essentially driven by a strong decline in

314   nanophytoplankton productivity whereas diatom productivity, even if contributing much less

315   to the total, remains relatively stable (except in the coastal Indian ocean). In contrast, in the

316   mid- and high-latitudes, diatoms are responsible for a large part of primary productivity

317   changes, and even become the main contributor to productivity changes in the highest

318   latitudes (> 60°S). This is consistent with increased nutrient availability in the highest

319   latitudes of the DO simulation due to the onset of the ACC. For instance, in the South Pacific,

320   even if winter convection zones are shallower and narrower, the enhanced nutrient supply

321   favours diatoms over nanophytoplankton.

322

323   **Discussion**

324   1. Comparison to model simulations

325   Numerous studies have investigated the role of DP on global climate, with varying

326   continental configurations [e.g., *Mikolajewicz et al.*, 1993; *Heinze and Crowley*, 1997;

327   *Toggweiler and Bjornsson*, 2000; *Sijp and England*, 2004; 2005; *Zhang et al.*, 2010; *Sijp et*

328   *al.*, 2011; *Yang et al.*, 2014; *England et al.*, 2017]. Of these, the most relevant simulations to

329   our study are those performed with the same continental configuration, in particular with the

330   Panama seaway open [e.g., *Mikolajewicz et al.*, 1993; *Yang et al.*, 2014; *Fyke et al.*, 2015].

331   Our reasoning here is based on the results of *Yang et al.* [2014] who demonstrated that the

332   impacts of DP are strongly dependant upon the configuration of the Panama seaway. Using

333   the CM2Mc model in a modern configuration (thus a closed Panama seaway), they show that

334   the closure of DP leads to an ocean circulation resembling that of modern, with the notable

335   exception of the suppression of the Antarctic Bottom Water cell in the Atlantic Ocean. This

336   result is broadly confirmed by *England et al.* [2017], in which the same experiment with the

337   fully coupled CSIRO Mk3L model demonstrates that the DP closed configuration exhibits

338   similar rates of NADW and AABW relative to modern. On the contrary, with an open

339   Panama seaway in an otherwise modern continental configuration, *Yang et al.* [2014] show

340   that the closure of DP generates a large and wide Southern overturning cell and suppresses

341   northern sinking. Our results, obtained with an open Panama seaway, are in agreement with

342   the findings of *Yang et al.* [2014], but also with those of *Fyke et al.* [2015] and *Mikolajewicz*

343   *et al.* [1993] who find a similar ocean circulation with a closed Drake – open Panama

344   configuration, albeit with simpler models (EMIC or ocean-only models).

345   Ocean circulation in the presence of an open DP and an open Panama seaway (i.e., the

346   impact of the opening of Panama) has also received considerable attention [e.g., *Mikolajewicz*

347   *et al.*, 1993; *Lunt et al.*, 2008; *Sepulchre et al.*, 2014; *Yang et al.*, 2014; *Fyke et al.*, 2015]. All

348   models ventilate the deep ocean from the South, although with reduced intensity than with a

349   closed DP, whereas the rates of deep-water formation in the North vary greatly between

350   studies. *Yang et al.* [2014] find virtually no difference between a DO configuration with or

351   without an open Panama seaway, that is, in both cases a strong NH deep overturning cell. In

352   their simulations with the UVic model, *Fyke et al.* [2015] obtain a significant reduction in

353   rates of NH deep water formation with an open Panama Gateway, albeit not a shutdown. A

354   similar result is obtained by *Sepulchre et al.* [2014] with the IPSL-CM4 model and by *Lunt et*

355   *al.* [2008] with the HadCM3 model. On the contrary, *Mikolajewicz et al.* [1993] find, with the

356   ocean-only Hamburg model, that a Drake open and Panama open configuration leads to the

357   cessation of the formation of NADW. In our runs, the thermohaline circulation induced by the

358   DO configuration shows a weak NH intermediate water formation, which is close to the no-

359   NADW state of *Mikolajewicz et al.* [1993]. It is interesting to note that the existence and

360   vigour of the NADW rates in these different models might, at least in part, be driven by the

361   geometry and size of the Panama gateway. Indeed, when Panama is closed (i.e. the modern

362   state), all models show NADW formation. Models run with an open but narrow Panama

363   seaway show reduced rates of NADW formation [*Lunt et al.*, 2008; *Sepulchre et al.*, 2014;

364   *Fyke et al.*, 2015] and those run with a wide Panama seaway show NADW shutdown

365   [*Mikolajewicz et al.*, 1993; this study]. Support for this finding comes from the simulations of

366   *Sijp et al.* [2009] and *Sijp et al.* [2011]. In the first of these studies, open and closed DP

367   simulations are performed in a modern continental configuration, that is, with a closed

368   Panama seaway. Their DP open simulations yield significant NADW formation. In the second

369   of these studies, coupled opening of DP and the Tasman gateway is simulated with the

370   Eocene configuration of *Huber et al.* [2003], which features a wide Panama seaway.

371   Interestingly, no NADW forms in these simulations. The simulations of *Yang et al.* [2014]

372   yield contrasting results, however, because, with DP open, vigorous NADW rates exist

373   regardless of whether a wide or a closed Panama seaway is prescribed. We tentatively infer

374   that the different boundary conditions (pCO_2 and ice sheets cover for instance) applied by

375   *Yang et al.* [2014] and in our study may play a role. In particular, the effect of pCO_2 on ocean

376   circulation may explain part of the discrepancy between the strong NADW rates found in the

377   fully coupled GCM used by *Yang et al.* [2014] and our weak intermediate water formation

378   state (see discussions in *Lunt et al.* [2010], *Donnadieu et al.* [2016] and *Winguth et al.*

379   [2012]). In this regard, it is also interesting to note that the no-NADW simulations of *Sijp et*

380   *al.* [2011] are run, as in our study, with elevated pCO_2. Another factor that should not be

381   ignored is that our fully coupled 1000 year GCM simulations can only be considered to have

382   reached quasi-equilibrium and may miss further reorganizations of ocean circulation.

383   However, although the Northern Hemisphere thermohaline state of the ocean differs between

384   studies, we note that the dynamical results produced by our simulations are consistent with

385   previous findings in that the opening of DP isolates Antarctica from warm and salty

386   subtropical waters, which acts to freshen and cool most of the surface Southern Ocean

387   (Supplementary Fig. 5). We conclude this climatic comparison by acknowledging that many

388   important studies involving the opening of DP (or Tasman gateway) have been carried out

389   using Eocene boundary conditions [e.g., *Huber et al.*, 2003; *Huber et al.*, 2004; *Huber and*

390   *Nof*, 2006; *Zhang et al.*, 2010; *Sijp et al.*, 2011] but the idealized character of our modelling

391   setup makes a direct comparison with these studies more questionable.

392   Two previous numerical studies are particularly relevant to our findings because they

393   numerically address the impact of gateways opening on the biogeochemical state of the ocean,

394   using the spatially resolved, albeit simpler, UVic climate-biogeochemical model [*Pagani et*

395   *al.*, 2011; *Fyke et al.*, 2015]. In line with the findings of *Fyke et al.* [2015] (their figure 9),

396   opening DP in our simulations increases DIC concentrations at depth in all basins although

397   we do not observe a shift from a higher Atlantic DIC concentration to a higher Pacific DIC

398   concentration (not shown). Our results also broadly agree with those of *Pagani et al.* [2011]

399 who show that the surface phosphate concentration in their Eocene simulation features a

400 spatially uniform increase in the low latitudes and decrease in the southern high latitudes

401 relative to modern, attributed to the shallower Eocene Southern Ocean upwelling cells relative

402 to modern induced by the gateways configurations. However, in our experiments, the changes

403 in surface nutrient concentrations in the southern high-latitudes are heterogeneous with areas

404 of increase and decrease. Because we can unambiguously attribute the reorganization of

405 surface nutrient concentration to DP opening in our simulations, we speculate that the

406 gateways impact in the work of *Pagani et al.* [2011] is intertwined with other drivers, such as

407 the much higher CO_2 concentration and other geographical characteristics imposed in their

408 Eocene run relative to their modern.

409

410 2. Comparison to observations

411   Many data studies have investigated paleoproductivity changes during the Eocene and

412 Oligocene [e.g., *Siesser*, 1995; *Diester-Haass and Zahn*, 1996; *Salamy and Zachos*, 1999;

413 *Diester-Haass and Zahn*, 2001; *Diester-Haass and Zachos*, 2003; *Nilsen et al.*, 2003;

414 *Schumacher and Lazarus*, 2004; *Dunkley Jones et al.*, 2008; *Griffith et al.*, 2010; *Coxall and*

415 *Wilson*, 2011; *Egan et al.*, 2013; *Moore et al.*, 2014; *Plancq et al.*, 2014; *Villa et al.*, 2014]

416 but the imprint of tectonics, particularly DP opening, is complex to decipher unambiguously

417 because other climatic shifts, such as the EOT glaciation, occur contemporaneously.

418 However, by investigating exclusively the effects of DP opening in a warmer world, our

419 simulations provide insights on this possible imprint. It is particularly interesting to note that,

420 when compared to records that span an interval longer than the EOT glaciation event, model

421 results are qualitatively consistent with data (Fig. 1), suggesting that, if the DP was

422 sufficiently well breached by the early Oligocene, at least part of the long-term

423 paleoproductivity signal recorded in the data may be attributed to its opening. Our results

424   suggest that DP opening drove a significant reduction in paleoproductivity in the low latitude

425   oceans – a finding consistent with long-term recorded changes, especially in the Eastern

426   Equatorial Pacific [*Schumacher and Lazarus*, 2004; *Moore et al.*, 2014] and in the Equatorial

427   Indian Ocean [*Siesser*, 1995]. In the high latitudes, most long-term records document an

428   increase in paleoproductivity [e.g., *Diester-Haass and Zahn*, 1996; 2001; *Schumacher and*

429   *Lazarus*, 2004], but the pattern of paleoproductivity increase/decrease simulated by the model

430   is not uniform and strongly related to variations in the convective mixing areas.

431   Our simple model-data comparison is similar to that of *Winguth et al.* [2012]. A more

432   in-depth analysis is unwarranted because we present a paleogeography sensitivity simulation

433   rather than an attempt to simulate Eocene-Oligocene events *sensu stricto*. Furthermore,

434   different data sets produce sometimes contrasting indications of paleoproductivity change

435   even when taken from the same site. A good example comes in the paleoproductivity records

436   from the Eastern Equatorial Pacific [e.g., *Coxall and Wilson*, 2011; *Erhardt et al.*, 2013;

437   *Moore et al.*, 2014]. Although there are reasonable explanations to these discrepancies

438   [*Erhardt et al.*, 2013; *Moore et al.*, 2014], this observation highlights the complexity

439   associated with reconstructing paleoproductivity from proxy signals [*Anderson and Delaney*,

440   2005]. In the high latitudes, many records show significant enhancement of the

441   paleoproductivity during the EOT event [e.g., *Salamy and Zachos*, 1999; *Diester-Haass and*

442   *Zahn*, 2001; *Plancq et al.*, 2014; *Villa et al.*, 2014] or during the latest Eocene [*Diekmann et*

443   *al.*, 2004; *Egan et al.*, 2013; *Villa et al.*, 2014]. In particular, during the latter, it has been

444   argued that pulses of tectonic opening of DP [*Scher and Martin*, 2006] may play a role in the

445   transition from oligotrophic to eutrophic nannofossils taxa [*Villa et al.*, 2014] or an increase

446   in diatom abundance [*Egan et al.*, 2013]. Based on Si isotopes records, *Egan et al.* [2013]

447   invoke increased diatom primary productivity to explain the recorded increased silicic acid

448   utilization at the surface at Site 1090. Although our modelled results support a net decrease in

449   diatoms (and nanophytoplankton) primary production in most of the South Atlantic Ocean

450   (Fig. 7), the simulated export production increases at Sites 689 [*Villa et al.*, 2014] and 1090

451   [*Egan et al.*, 2013]. Primary and export productivity do indeed not necessarily co-vary as

452   organic matter remineralization, among others, is a function of temperature [*John et al.*,

453   2013]. The significant modelled surface cooling when DP opens at Sites 689 and 1090

454   (Supplementary Fig. 5) generates reduced recycling of organic matter and may thus explain

455   the contrasting variations of primary and export productivity.

456

457   3. Caveats related to the idealized framework of the study

458   Taken at face value, our simulated paleoproductivity changes fit marine records

459   reasonably well, but important caveats must be kept in mind when interpreting our model

460   results. First, we do not use a realistic late Eocene global paleogeography, either regarding the

461   geometry of important gateways or other major tectonic differences such as the existence of

462   the Tethys Sea or the position and height of the Tibetan Plateau. Our idealized simulations

463   therefore remain a sensitivity experiment to the opening of DP. Because our simulated

464   paleoproductivity changes are essentially driven by the onset of the ACC, the impact of a

465   closed or restricted Tasman seaway prior to the latest Eocene [*Huber et al.*, 2004; *Stickley et*

466   *al.*, 2004] may have important consequences for paleoproductivity patterns. However, a

467   recent idealized study suggests that a circumpolar water path, which would circumvent

468   Australia, could exist even in the absence of an open Tasman seaway [*Munday et al.*, 2015].

469   Second, our simulations were performed using two end-member boundary conditions (DP

470   closed and DP open) that are not strictly representative of the late Eocene and Oligocene, as

471   some evidence points to initial opening of DP as early as the Early Eocene [*Eagles et al.*,

472   2006; *Eagles and Jokat*, 2014]. The climatic relevance of an incipient opening is intuitively

473   questionable and the concept of a threshold relationship between gateway opening and

474 climate response is appealing. *Sijp and England* [2005] argued that the sill depth of DP

475 critically impacted the global ocean circulation, because it was instrumental in controlling the

476 formation of NADW, but this result was obtained with a closed Panama Seaway, which is a

477 configuration that favours NADW formation [*Lunt et al.*, 2008; *Sepulchre et al.*, 2014; *Yang*

478 *et al.*, 2014]. The open Panama simulations performed here are not sufficient to

479 unambiguously answer this question. Finally, our offline PISCES simulations are run with

480 fixed nutrient supply from rivers, which are unaffected by variations in runoff whereas we

481 know that changes in nutrient and carbonate supply down rivers across the Eocene Oligocene

482 Transition are both likely and capable of driving major change in global carbon cycling

483 [*Coxall et al.*, 2005; *Dunkley Jones et al.*, 2008; *Merico et al.*, 2008; *Armstrong McKay et al.*,

484 2016].

485

486 **Conclusion**

487 Using the IPSL-CM5A coupled model we have shown that the opening of Drake

488 Passage profoundly alters oceanic paleoproductivity patterns across the globe. The

489 reorganization of the oceanic circulation, from a well-ventilated ocean when Drake Passage is

490 closed to a more stagnant state when Drake Passage is open, drives subsurface nutrient

491 depletion in the low latitudes. Nanophytoplankton, rather than diatoms – possibly because the

492 latter are only marginal contributors to the modelled low latitude primary productivity, are

493 strongly affected by this depletion and the productivity consequently declines, especially in

494 the Pacific and Indian oceans. In the high latitudes, productivity changes are driven both by

495 nutrient availability and areas of convective mixing, which generate zones of productivity

496 increase (most of the southern Pacific and Indian oceans) and decrease (most of the South

497 Atlantic Ocean). In contrast to the low latitudes, diatoms are largely responsible for these

498 productivity variations, especially in the southernmost latitudes. A simple qualitative

499 comparison with geological records reveals a good match between locations of

500 paleoproductivity changes simulated by the model and inferred from data, suggesting that the

501 role of Drake Passage opening in driving part of the long-term productivity signal across the

502 late Eocene and early Oligocene may be non-negligible.

503

504

505

506

507

508

509

510

511

512

513

514

515

516

517

518

519

520

521

522

523

Acknowledgements

Author Contributions

J.-B.L. designed and performed the numerical simulations, with contributions from Y.D., and wrote the draft of the manuscript. All authors analysed and discussed the results and contributed to the final version of the manuscript.

Additional Information

The authors declare no competing financial interest. Correspondence and requests for materials should be addressed to either J.-B.L. (jbladant@gmail.com) or Y.D. (donnadieu@cerege.fr).

References

Anderson, L. D., and M. L. Delaney (2005), Middle Eocene to early Oligocene paleoceanography from Agulhas Ridge, Southern Ocean (Ocean Drilling Program Leg 177, Site 1090), *Paleoceanography*, *20*(1).

Armstrong McKay, D. I., T. Tyrrell, and P. A. Wilson (2016), Global carbon cycle perturbation across the Eocene‐Oligocene climate transition, *Paleoceanography*.

Aumont, O., and L. Bopp (2006), Globalizing results from ocean in situ iron fertilization studies, *Global Biogeochemical Cycles*, *20*(2).

Barker, P., and J. Burrell (1977), The opening of Drake passage, *Marine geology*, *25*(1), 15-34.

Barker, P. F., G. M. Filippelli, F. Florindo, E. E. Martin, and H. D. Scher (2007), Onset and role of the Antarctic Circumpolar Current, *Deep Sea Research Part II: Topical Studies in Oceanography*, *54*(21), 2388-2398.

Beerling, D. J., and D. L. Royer (2011), Convergent Cenozoic CO2 history, *Nature Geoscience*, *4*(7), 418-420.

Bopp, L., L. Resplandy, J. C. Orr, S. C. Doney, J. P. Dunne, M. Gehlen, P. Halloran, C. Heinze, T. Ilyina, and R. Seferian (2013), Multiple stressors of ocean ecosystems in the 21st century: projections with CMIP5 models, *Biogeosciences*, *10*, 6225-6245.

Contoux, C., C. Dumas, G. Ramstein, A. Jost, and A. M. Dolan (2015), Modelling Greenland ice sheet inception and sustainability during the Late Pliocene, *Earth and Planetary Science Letters*, *424*, 295-305.

Coxall, H. K., and P. A. Wilson (2011), Early Oligocene glaciation and productivity in the eastern equatorial Pacific: Insights into global carbon cycling, *Paleoceanography*, *26*(2).

Coxall, H. K., P. A. Wilson, H. Pälike, C. H. Lear, and J. Backman (2005), Rapid stepwise onset of Antarctic glaciation and deeper calcite compensation in the Pacific Ocean, *Nature*, *433*(7021), 53-57.

Dalziel, I. W. D., L. A. Lawver, J. A. Pearce, P. F. Barker, A. R. Hastie, D. N. Barfod, H. W. Schenke, and M. B. Davis (2013), A potential barrier to deep Antarctic circumpolar flow until the late Miocene?, *Geology*, *41*(9), 947-950.

DeConto, R. M., and D. Pollard (2003), Rapid Cenozoic glaciation of Antarctica induced by declining atmospheric CO2, *Nature*, *421*, 245-249.

Diekmann, B., G. Kuhn, R. Gersonde, and A. Mackensen (2004), Middle Eocene to early Miocene environmental changes in the sub-Antarctic Southern Ocean: evidence from biogenic and terrigenous depositional patterns at ODP Site 1090, *Global and Planetary Change*, *40*(3), 295-313.

Diester-Haass, L., and R. Zahn (1996), Eocene-Oligocene transition in the Southern Ocean: History of water mass circulation and biological productivity, *Geology*, *24*(2), 163-166.

Diester-Haass, L., and R. Zahn (2001), Paleoproductivity increase at the Eocene‚ÄìOligocene climatic transition: ODP/DSDP Sites 763 and 592, *Palaeogeography, Palaeoclimatology, Palaeoecology*, *172*(1), 153-170.

Diester-Haass, L., and J. Zachos (2003), The Eocene-Oligocene transition in the Equatorial Atlantic (ODP Site 925); paleoproductivity increase and positive d13C excursion., in *From greenhouse to icehouse; the marine Eocene-Oligocene transition*, edited by D. R. Prothero, L. C. Ivany and E. A. Nesbitt, Columbia University Press, New York, NY, USA.

595   Donnadieu, Y., E. Pucéat, M. Moiroud, F. Guillocheau, and J.-F. Deconinck (2016), A
596   better-ventilated ocean triggered by Late Cretaceous changes in continental
597   configuration, *Nature communications*, *7*.
598   Dufresne, J. L., et al. (2013), Climate change projections using the IPSL-CM5 Earth
599   System Model: from CMIP3 to CMIP5, *Climate Dynamics*, *40*(9-10), 2123-2165.
600   Dunkley Jones, T., P. R. Bown, P. N. Pearson, B. S. Wade, H. K. Coxall, and C. H. Lear
601   (2008), Major shifts in calcareous phytoplankton assemblages through the Eocene‐
602   Oligocene transition of Tanzania and their implications for low‐latitude primary
603   production, *Paleoceanography*, *23*(4).
604   Eagles, G., and W. Jokat (2014), Tectonic reconstructions for paleobathymetry in Drake
605   Passage, *Tectonophysics*, *611*, 28-50.
606   Eagles, G., R. Livermore, and P. Morris (2006), Small basins in the Scotia Sea: the Eocene
607   Drake passage gateway, *Earth and Planetary Science Letters*, *242*(3), 343-353.
608   Egan, K. E., R. E. M. Rickaby, K. R. Hendry, and A. N. Halliday (2013), Opening the
609   gateways for diatoms primes Earth for Antarctic glaciation, *Earth and Planetary Science
610   Letters*, *375*, 34-43.
611   Elsworth, G., E. Galbraith, G. Halverson, and S. Yang (2017), Enhanced weathering and
612   CO2 drawdown caused by latest Eocene strengthening of the Atlantic meridional
613   overturning circulation, *Nature Geoscience*, *10*(3), 213-216.
614   England, M. H., D. K. Hutchinson, A. Santoso, and W. P. Sijp (2017), Ice-atmosphere
615   feedbacks dominate the response of the climate system to Drake Passage closure,
616   *Journal of Climate*(2017).
617   Erhardt, A. M., H. Pälike, and A. Paytan (2013), High‐resolution record of export
618   production in the eastern equatorial Pacific across the Eocene‐Oligocene transition
619   and relationships to global climatic records, *Paleoceanography*, *28*(1), 130-142.
620   Faul, K. L., and M. L. Delaney (2010), A comparison of early Paleogene export
621   productivity and organic carbon burial flux for Maud Rise, Weddell Sea, and Kerguelen
622   Plateau, south Indian Ocean, *Paleoceanography*, *25*(3).
623   Ferreira, D., J. Marshall, and J.-M. Campin (2010), Localization of deep water formation:
624   Role of atmospheric moisture transport and geometrical constraints on ocean
625   circulation, *Journal of Climate*, *23*(6), 1456-1476.
626   Fichefet, T., and M. A. Morales Maqueda (1997), Sensitivity of a global sea ice model to
627   the treatment of ice thermodynamics and dynamics, *Journal of Geophysical Research:
628   Oceans (1978–2012)*, *102*(C6), 12609-12646.
629   Fyke, J. G., M. D'Orgeville, and A. J. Weaver (2015), Drake Passage and Central American
630   Seaway controls on the distribution of the oceanic carbon reservoir, *Global and
631   Planetary Change*, *128*, 72-82.
632   Gasson, E., et al. (2014), Uncertainties in the modelled CO2 threshold for Antarctic
633   glaciation, *Climate of the Past*, *10*(2), 451-466.
634   Goldner, A., N. Herold, and M. Huber (2014), Antarctic glaciation caused ocean
635   circulation changes at the Eocene-Oligocene transition, *Nature*, *511*(7511), 574-577.
636   Griffith, E., M. Calhoun, E. Thomas, K. Averyt, A. Erhardt, T. Bralower, M. Lyle, A.
637   Olivarez‐Lyle, and A. Paytan (2010), Export productivity and carbonate accumulation
638   in the Pacific Basin at the transition from a greenhouse to icehouse climate (late Eocene
639   to early Oligocene), *Paleoceanography*, *25*(3).
640   Hain, M. P., D. M. Sigman, and G. H. Haug (2014), 8.18 The Biological Pump in the Past,
641   *Reference Module in Earth Systems and Environmental Sciences, Treatise on Geochemistry*,
642   485-517.

Heinze, C., and T. J. Crowley (1997), Sedimentary response to ocean gateway circulation changes, *Paleoceanography*, *12*(6), 742-754.

Heureux, A. M. C., and R. E. M. Rickaby (2015), Refining our estimate of atmospheric CO2 across the Eocene–Oligocene climatic transition, *Earth and Planetary Science Letters*, *409*, 329-338.

Hourdin, F., M.-A. Foujols, F. Codron, V. Guemas, J.-L. Dufresne, S. Bony, S. Denvil, L. Guez, F. Lott, and J. Ghattas (2013), Impact of the LMDZ atmospheric grid configuration on the climate and sensitivity of the IPSL-CM5A coupled model, *Climate Dynamics*, *40*(9-10), 2167-2192.

Huber, M., and D. Nof (2006), The ocean circulation in the southern hemisphere and its climatic impacts in the Eocene, *Palaeogeography, Palaeoclimatology, Palaeoecology*, *231*(1), 9-28.

Huber, M., L. C. Sloan, and C. Shellito (2003), Early Paleogene oceans and climate: A fully coupled modeling approach using the NCAR CCSM, *Geological Society of America Special Papers*, *369*, 25-47.

Huber, M., H. Brinkhuis, C. E. Stickley, K. Döös, A. Sluijs, J. Warnaar, S. A. Schellenberg, and G. L. Williams (2004), Eocene circulation of the Southern Ocean: Was Antarctica kept warm by subtropical waters?, *Paleoceanography*, *19*(4), PA4026.

John, E. H., P. N. Pearson, H. K. Coxall, H. Birch, B. S. Wade, and G. L. Foster (2013), Warm ocean processes and carbon cycling in the Eocene, *Phil. Trans. R. Soc. A*, *371*(2001), 20130099.

Kageyama, M., et al. (2013), Mid-Holocene and Last Glacial Maximum climate simulations with the IPSL model—part I: comparing IPSL_CM5A to IPSL_CM4, *Climate Dynamics*, *40*(9-10), 2447-2468.

Katz, M. E., B. S. Cramer, J. R. Toggweiler, G. Esmay, C. Liu, K. G. Miller, Y. Rosenthal, B. S. Wade, and J. D. Wright (2011), Impact of Antarctic Circumpolar Current Development on Late Paleogene Ocean Structure, *Science*, *332*(6033), 1076-1079.

Kennett, J. P. (1977), Cenozoic evolution of Antarctic glaciation, the circum-Antarctic Ocean, and their impact on global paleoceanography, *Journal of Geophysical Research*, *82*(27), 3843-3860.

Krinner, G., N. Viovy, N. de Noblet‐Ducoudré, J. Ogée, J. Polcher, P. Friedlingstein, P. Ciais, S. Sitch, and I. C. Prentice (2005), A dynamic global vegetation model for studies of the coupled atmosphere‐biosphere system, *Global Biogeochemical Cycles*, *19*(1).

Ladant, J.-B., Y. Donnadieu, V. Lefebvre, and C. Dumas (2014), The respective role of atmospheric carbon dioxide and orbital parameters on ice sheet evolution at the Eocene-Oligocene transition, *Paleoceanography*, *29*(8), 810-823.

Lagabrielle, Y., Y. Goddéris, Y. Donnadieu, J. Malavieille, and M. Suarez (2009), The tectonic history of Drake Passage and its possible impacts on global climate, *Earth and Planetary Science Letters*, *279*(3-4), 197-211.

Le Mézo, P., L. Beaufort, L. Bopp, P. Braconnot, and M. Kageyama (2017), From monsoon to marine productivity in the Arabian Sea: insights from glacial and interglacial climates, *Climate of the Past*, *13*(7), 759-778.

Lear, C. H., and D. J. Lunt (2016), How Antarctica got its ice, *Science*, *352*(6281), 34-35.

Lear, C. H., H. Elderfield, and P. A. Wilson (2000), Cenozoic deep-sea temperatures and global ice volumes from Mg/Ca in benthic foraminiferal calcite, *Science*, *287*(5451), 269-272.

Lunt, D. J., P. J. Valdes, A. Haywood, and I. C. Rutt (2008), Closure of the Panama Seaway during the Pliocene: implications for climate and Northern Hemisphere glaciation, *Climate Dynamics*, *30*(1), 1-18.

692 Lunt, D. J., P. J. Valdes, T. D. Jones, A. Ridgwell, A. M. Haywood, D. N. Schmidt, R. Marsh,
693 and M. Maslin (2010), CO2-driven ocean circulation changes as an amplifier of
694 Paleocene-Eocene thermal maximum hydrate destabilization, *Geology*, *38*(10), 875-878.

695 Madec, G. (2008), NEMO ocean engine. Technical note.*Rep.*, IPSL.

696 Madec, G., and M. Imbard (1996), A global ocean mesh to overcome the North Pole
697 singularity, *Climate Dynamics*, *12*(6), 381-388.

698 Mariotti, V., L. Bopp, A. Tagliabue, M. Kageyama, and D. Swingedouw (2012), Marine
699 productivity response to Heinrich events: a model-data comparison, *Climate of the Past*,
700 *8*(5), 1581.

701 Matthews, R. K., and R. Z. Poore (1980), Tertiary δ 18O record and glacio-eustatic sea-
702 level fluctuations, *Geology*, *8*(10), 501-504.

703 Merico, A., T. Tyrrell, and P. A. Wilson (2008), Eocene/Oligocene ocean de-acidification
704 linked to Antarctic glaciation by sea-level fall, *Nature*, *452*(7190), 979-982.

705 Mikolajewicz, U., E. Maier-Reimer, T. J. Crowley, and K.-Y. Kim (1993), Effect of Drake
706 and Panamanian gateways on the circulation of an ocean model, *Paleoceanography*, *8*(4),
707 409-426.

708 Miller, K. G., J. D. Wright, and R. G. Fairbanks (1991), Unlocking the ice house:
709 Oligocene‐Miocene oxygen isotopes, eustasy, and margin erosion, *Journal of
710 Geophysical Research: Solid Earth*, *96*(B4), 6829-6848.

711 Moore, T. C., B. S. Wade, T. Westerhold, A. M. Erhardt, H. K. Coxall, J. Baldauf, and M.
712 Wagner (2014), Equatorial Pacific productivity changes near the Eocene‐Oligocene
713 boundary, *Paleoceanography*, *29*(9), 825-844.

714 Munday, D. R., H. L. Johnson, and D. P. Marshall (2015), The role of ocean gateways in the
715 dynamics and sensitivity to wind stress of the early Antarctic Circumpolar Current,
716 *Paleoceanography*, *30*(3), 284-302.

717 Nilsen, E. B., L. D. Anderson, and M. L. Delaney (2003), Paleoproductivity, nutrient burial,
718 climate change and the carbon cycle in the western equatorial Atlantic across the
719 Eocene/Oligocene boundary, *Paleoceanography*, *18*(3).

720 Pagani, M., M. Huber, Z. Liu, S. M. Bohaty, J. Henderiks, W. Sijp, S. Krishnan, and R. M.
721 DeConto (2011), The Role of Carbon Dioxide During the Onset of Antarctic Glaciation,
722 *Science*, *334*(6060), 1261-1264.

723 Pälike, H., et al. (2012), A Cenozoic record of the equatorial Pacific carbonate
724 compensation depth, *Nature*, *488*(7413), 609-614.

725 Pearson, P. N., G. L. Foster, and B. S. Wade (2009), Atmospheric carbon dioxide through
726 the Eocene–Oligocene climate transition, *Nature*, *461*(7267), 1110-1113.

727 Plancq, J., E. Mattioli, B. Pittet, L. Simon, and V. Grossi (2014), Productivity and sea-
728 surface temperature changes recorded during the late Eocene–early Oligocene at DSDP
729 Site 511 (South Atlantic), *Palaeogeography, Palaeoclimatology, Palaeoecology*, *407*, 34-
730 44.

731 Salamy, K. A., and J. C. Zachos (1999), Latest Eocene–Early Oligocene climate change and
732 Southern Ocean fertility: inferences from sediment accumulation and stable isotope
733 data, *Palaeogeography, Palaeoclimatology, Palaeoecology*, *145*(1), 61-77.

734 Sarmiento, J. L., N. Gruber, M. A. Brzezinski, and J. P. Dunne (2004), High-latitude
735 controls of thermocline nutrients and low latitude biological productivity, *Nature*,
736 *427*(6969), 56-60.

737 Scher, H., and E. Martin (2006), Timing and climatic consequences of the opening of
738 Drake Passage, *Science*, *312*(5772), 428-430.

739   Scher, H., J. M. Whittaker, S. E. Williams, J. C. Latimer, W. E. Kordesch, and M. L. Delaney
740   (2015), Onset of Antarctic Circumpolar Current 30 million years ago as Tasmanian
741   Gateway aligned with westerlies, *Nature*, *523*(7562), 580-583.
742   Schumacher, S., and D. Lazarus (2004), Regional differences in pelagic productivity in
743   the late Eocene to early Oligocene—a comparison of southern high latitudes and lower
744   latitudes, *Palaeogeography, palaeoclimatology, palaeoecology*, *214*(3), 243-263.
745   Séférian, R., et al. (2016), Inconsistent strategies to spin up models in CMIP5:
746   implications for ocean biogeochemical model performance assessment, *Geoscientific
747   Model Development*, *9*(5), 1827-1851.
748   Sepulchre, P., T. Arsouze, Y. Donnadieu, J. C. Dutay, C. Jaramillo, J. Le Bras, E. Martin, C.
749   Montes, and A. J. Waite (2014), Consequences of shoaling of the Central American
750   Seaway determined from modeling Nd isotopes, *Paleoceanography*, *29*(3), 176-189.
751   Siesser, W. G. (1995), Paleoproductivity of the Indian Ocean during the Tertiary period,
752   *Global and Planetary Change*, *11*(1-2), 71-88.
753   Sijp, W. P., and M. H. England (2004), Effect of the Drake Passage throughflow on global
754   climate, *Journal of physical oceanography*, *34*(5), 1254-1266.
755   Sijp, W. P., and M. H. England (2005), Role of the Drake Passage in controlling the
756   stability of the ocean's thermohaline circulation, *Journal of climate*, *18*(12), 1957-1966.
757   Sijp, W. P., M. H. England, and J. R. Toggweiler (2009), Effect of ocean gateway changes
758   under greenhouse warmth, *Journal of Climate*, *22*(24), 6639-6652.
759   Sijp, W. P., M. H. England, and M. Huber (2011), Effect of the deepening of the Tasman
760   Gateway on the global ocean, *Paleoceanography*, *26*(4), PA4207.
761   Stickley, C. E., H. Brinkhuis, S. A. Schellenberg, A. Sluijs, U. Röhl, M. Fuller, M. Grauert, M.
762   Huber, J. Warnaar, and G. L. Williams (2004), Timing and nature of the deepening of the
763   Tasmanian Gateway, *Paleoceanography*, *19*(4), PA4027
764   Tagliabue, A., O. Aumont, and L. Bopp (2014), The impact of different external sources of
765   iron on the global carbon cycle, *Geophysical Research Letters*, *41*(3), 920-926.
766   Takahashi, T., W. S. Broecker, and S. Langer (1985), Redfield ratio based on chemical
767   data from isopycnal surfaces, *Journal of Geophysical Research: Oceans*, *90*(C4), 6907-
768   6924.
769   Tan, N., G. Ramstein, C. Dumas, C. Contoux, J.-B. Ladant, P. Sepulchre, Z. Zhang, and S. De
770   Schepper (2017), Exploring the MIS M2 glaciation occurring during a warm and high
771   atmospheric CO2 Pliocene background climate, *Earth and Planetary Science Letters*, *472*,
772   266-276.
773   Toggweiler, J., and H. Bjornsson (2000), Drake Passage and palaeoclimate, *Journal of
774   Quaternary Science*, *15*(4), 319-328.
775   Toggweiler, J. R., and B. Samuels (1993), New radiocarbon constraints on the upwelling
776   of abyssal water to the ocean's surface., in *The global carbon cycle.*, edited by M.
777   Heimann, pp. 333-366, Springer, Berlin, Heidelberg.
778   Valcke, S. (2006), OASIS user's guide (prism-2.5). Tech. Rep. TR/CMGC/06/73, PRISM
779   Report No3.*Rep.*, CERFACS, Toulouse, France.
780   Villa, G., C. Fioroni, D. Persico, A. P. Roberts, and F. Florindo (2014), Middle Eocene to
781   Late Oligocene Antarctic glaciation/deglaciation and southern ocean productivity,
782   *Paleoceanography*, *29*(3), 223-237.
783   Winguth, A. M. E., E. Thomas, and C. Winguth (2012), Global decline in ocean ventilation,
784   oxygenation, and productivity during the Paleocene-Eocene Thermal Maximum:
785   Implications for the benthic extinction, *Geology*, *40*(3), 263-266.
786   Yang, S., E. Galbraith, and J. Palter (2014), Coupled climate impacts of the Drake Passage
787   and the Panama Seaway, *Climate Dynamics*, *43*(1-2), 37-52.

788 Zachos, J. C., and L. R. Kump (2005), Carbon cycle feedbacks and the initiation of
789 Antarctic glaciation in the earliest Oligocene, *Global and Planetary Change*, *47*(1), 51-66.
790 Zhang, Z.-S., Q. Yan, and H.-J. Wang (2010), Has the Drake passage played an essential
791 role in the Cenozoic cooling, *Atmos. Oceanic Sci. Lett*, *3*(5), 288-292.

792

793

794 **Legends and Tables**

795

Site (Reference)	Latitude	Longitude	Qualitative productivity change
1209-1211 (Griffith et al. 2010)	~ 20°N	~ 172°W	decrease
925 (Nilsen et al. 2003) *	~ 4°N	~ 43°W	no change
U1333 (Moore et al. 2014)	~ 3°N	~ 113°W	decrease
1218 and U1334 (Moore et al. 2014)	~ 0-2°N	~ 110°W	decrease
462 (Schumacher and Lazarus 2004)	~ 2°S	~ 178°W	no change
959 (Schumacher and Lazarus 2004)	~ 2°S	~ 13°W	slight decrease or no change
574 (Schumacher and Lazarus 2004)	~ 7°S	~ 117°W	slight decrease or no change
709 (Siesser 1995)	~ 10°S	~ 75°E	decrease
758 (Siesser 1995)	~ 10°S	~ 110°E	no change or no data
757 (Siesser 1995)	~ 30°S	~ 95°E	no change
762 (Siesser 1995)	~ 35°S	~ 115°E	decrease
763 (Diester-Haas and Zahn 2001)	~ 40°S	~ 112°E	increase
1090 (Diekmann et al. 2004)	~ 43°S	~ 9°E	decrease
1090 (Egan et al. 2013)	~ 43°S	~ 9°E	increase
752 (Siesser 1995)	~ 45°S	~ 90°E	no change or no data
511 (Plancq et al. 2014)	~ 52°S	~ 42°W	increase
511 (Schumacher and Lazarus 2004)	~ 55°S	~ 42°W	increase
748 (Siesser 1995)	~ 55°S	~ 70°E	no change or no data
592 (Diester-Haas and Zahn 2001)	~ 55°S	~ 165°E	increase
748 (Schumacher and Lazarus 2004)	~ 56°S	~ 73°E	increase
748 (Villa et al. 2014)	~ 57°S	~ 74°E	increase
738 and 744 (Villa et al. 2014) *	~ 63°S	~ 83°E	increase
689 (Schumacher and Lazarus 2004)	~ 72°S	~ 15°W	increase
689 and 690 (Villa et al. 2014)	~ 72°S	~ 15°W	increase

Table 1. Compilation of long-term productivity changes across the late Eocene and early Oligocene. Longitudes and latitudes are approximate paleolocations of the sites. The asterisk denotes sites where modern location is used. There are a few redundant sites but findings from different studies at these sites are similar.

796

797

798   **Figure 1.** (top) Mean annual export production at 100 m (gC.m^{-2}.yr^{-1}) for DC and DO
799   simulations. (bottom) Annual export production at 100 m difference between DO and DC
800   (gC.m^{-2}.yr^{-1}). Color-coded circles represent productivity variations from data records (see
801   Table 1): red = increase, blue = decrease, pale shading = weak or uncertain variations, white =
802   no variations or lack of data.
803

804

805   **Figure 2.** Zonally averaged export production at 100 m (gC.m^{-2}.yr^{-1}) at the global scale and in
806   each basin for DC (black solid lines) and DO (red dashed lines).
807

808

809   **Figure 3.** (top) Mean annual zonally averaged nitrate concentration (µmol.L^{-1}) for DC and
810   DO with density contours (0.1 kg.m^{-3}) overlain. (bottom) Mean annual zonally averaged
811   nitrate concentration difference (µmol.L^{-1}) between DO and DC, with density contours (0.1
812   kg.m^{-3}) overlain in black for DC and green for DO. Note that 1000 kg.m^{-3} is subtracted from
813   density values on the plot.
814

815

816   **Figure 4.** Global, Atlantic, Pacific and Indian upper 500 m nitrate concentration gradients in
817   the low latitudes (40°S – 40°N, solid lines) and the southern high latitudes (90°S – 60°S,
818   dashed lines) for DC (black) and DO (red).
819

820

821   **Figure 5.** Global meridional overturning streamfunction (Sv, clockwise positive) for DC and
822   DO. Contours 4 Sv, negative dashed.
823

824

825   **Figure 6.** Wintertime deep-water formation in the Southern (top) and Northern (bottom)
826   Hemispheres for DF and DO simulations, as represented by the ocean mixed-layer depth (m).
827   Note that the scale differs between southern and northern plots.
828

829

830   **Figure 7.** Diatoms and nanophytoplankton primary production difference (gC.m^{-2}.yr^{-1})
831   between DO and DC.
832

833

834   **Figures**

Figure 1.

835

836

837

838

839

840

Figure 2.

841

Figure 3.

Figure 4.

846

847

848

849

850

851

852

853

854

855

Figure 5.

856

857

858

859

860

861

862

863

864

865

866

867

868

869

870

871

872

Drake Closed   Drake Open

Mixed−Layer Depth (m)

0   800   1600   2400   3200

Mixed−Layer Depth (m)

0   200   400   600   800
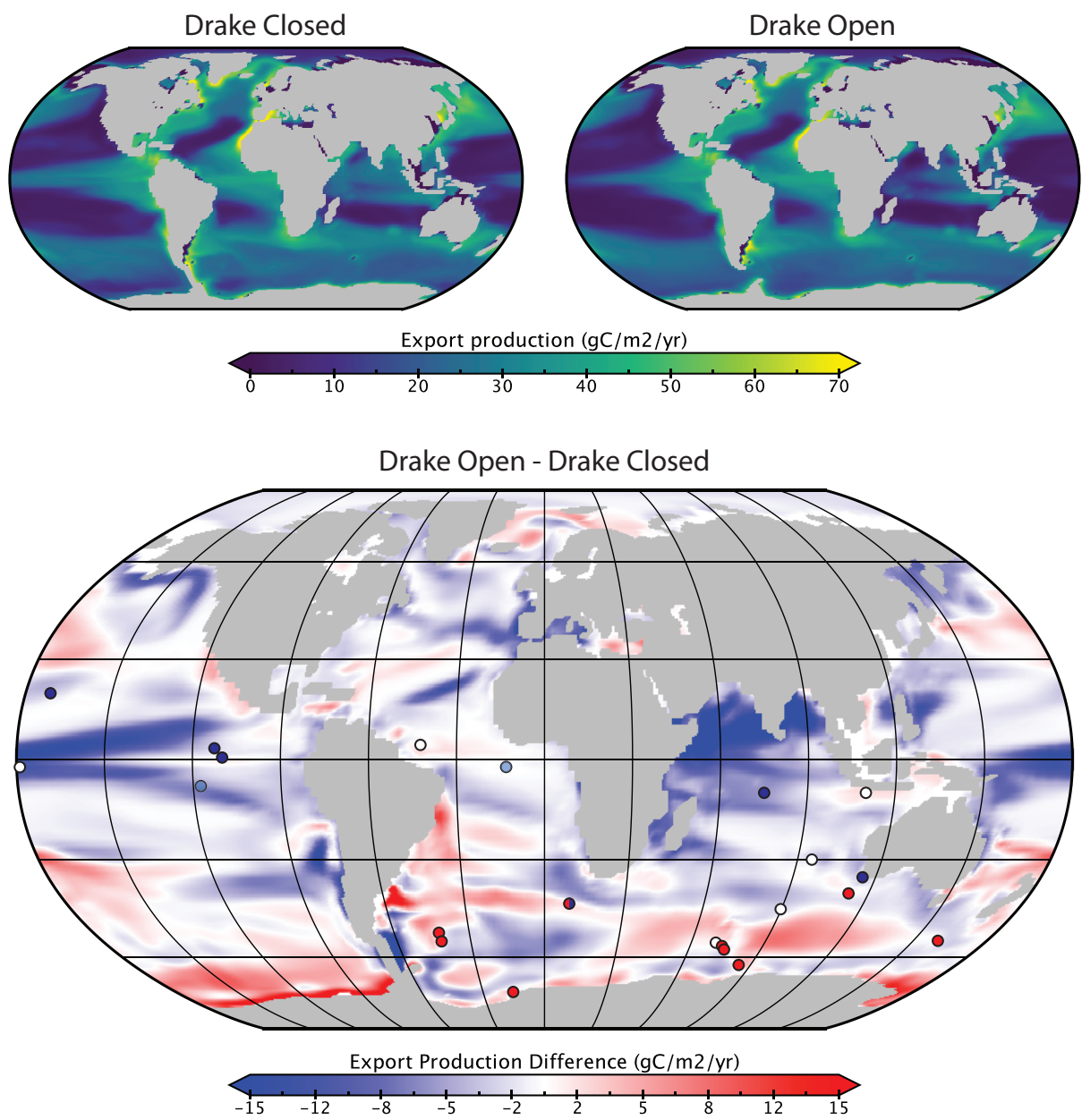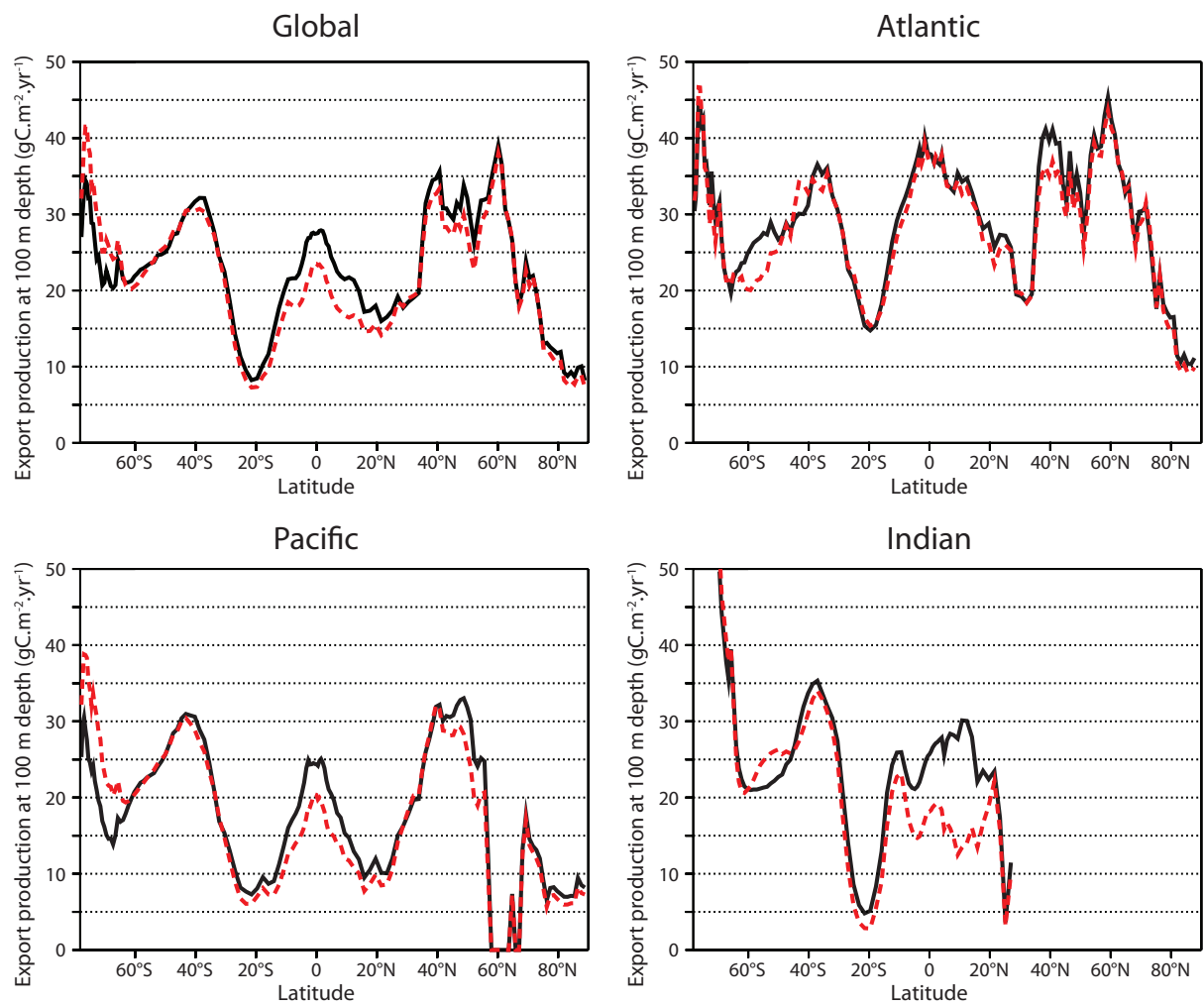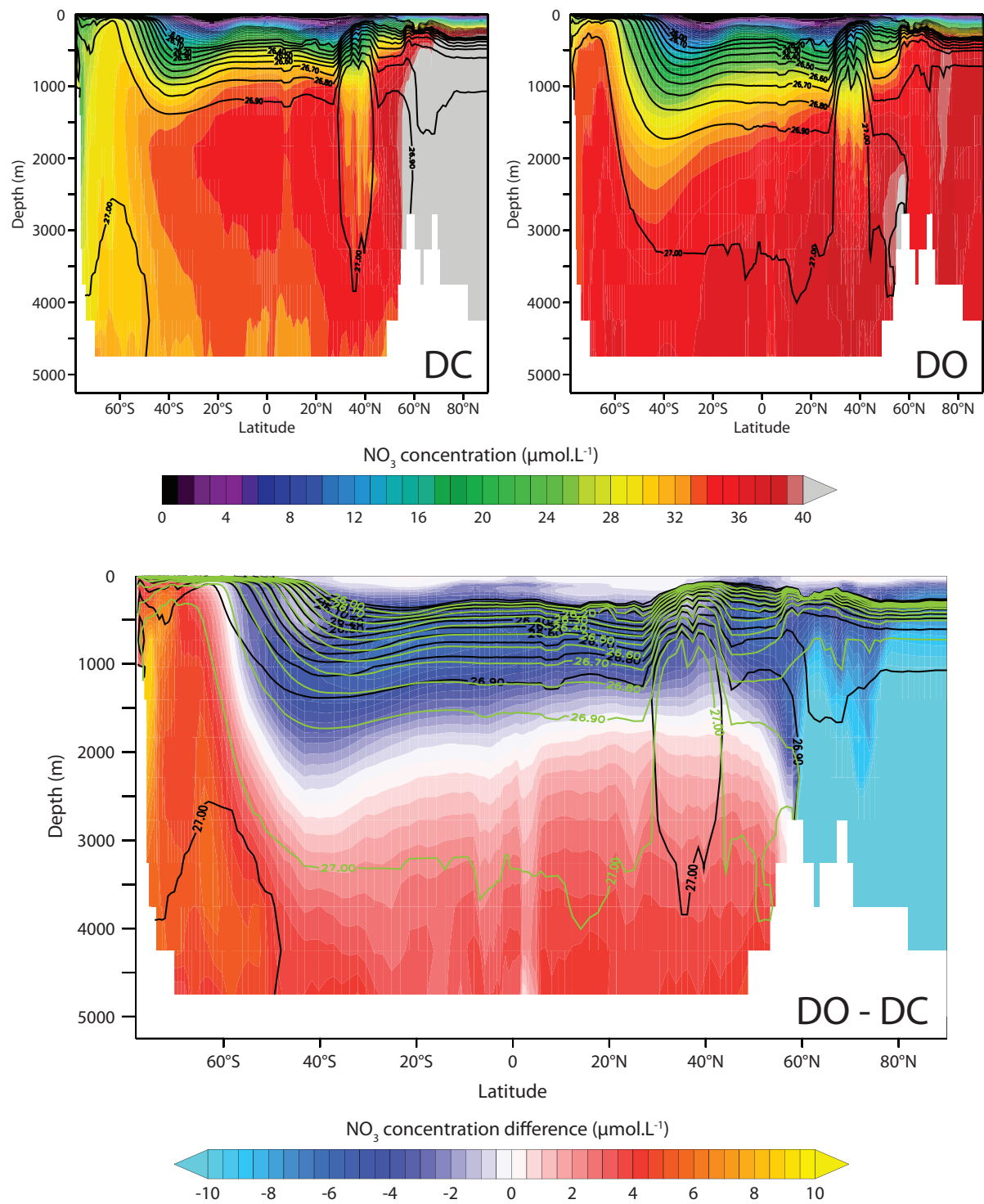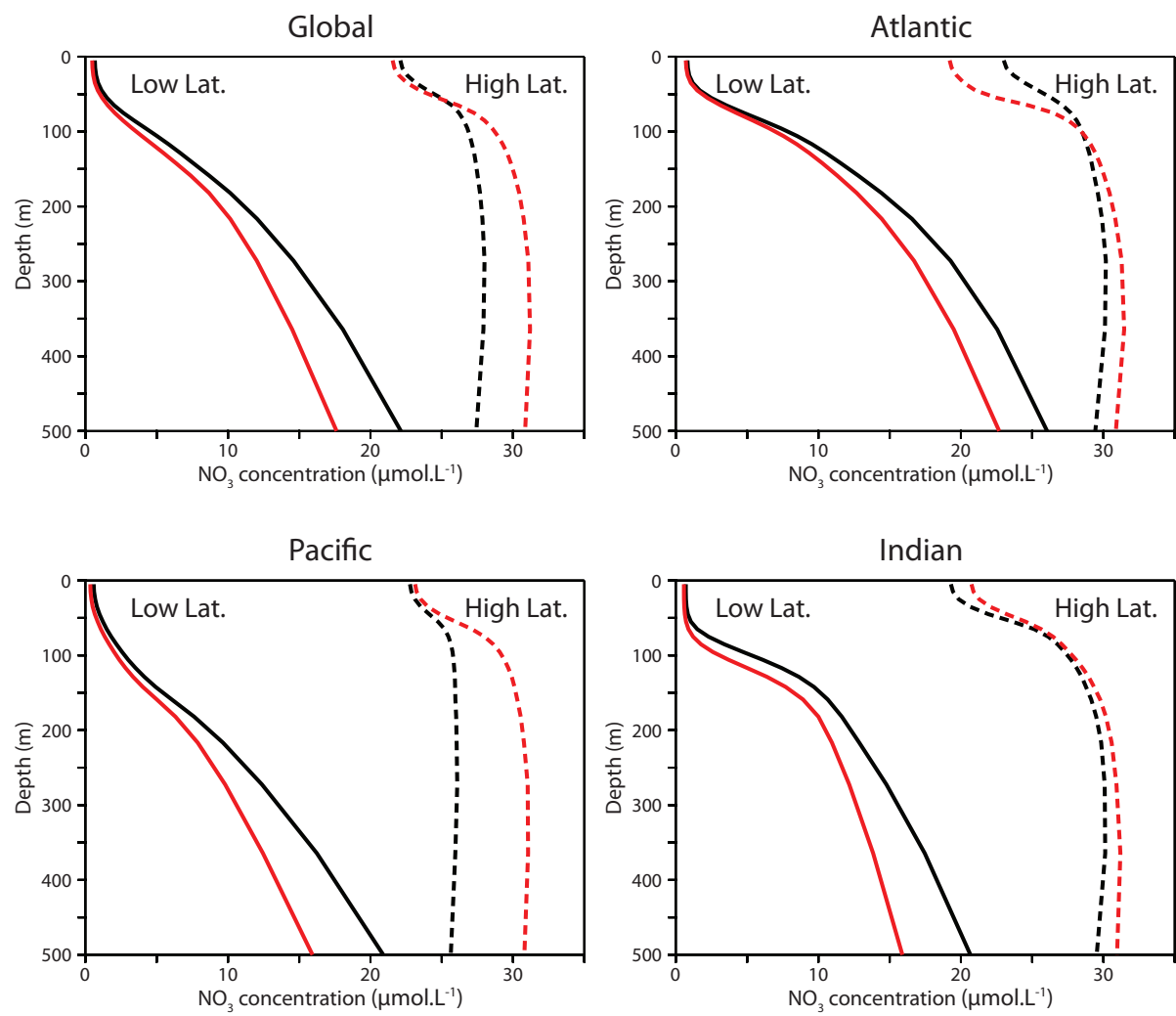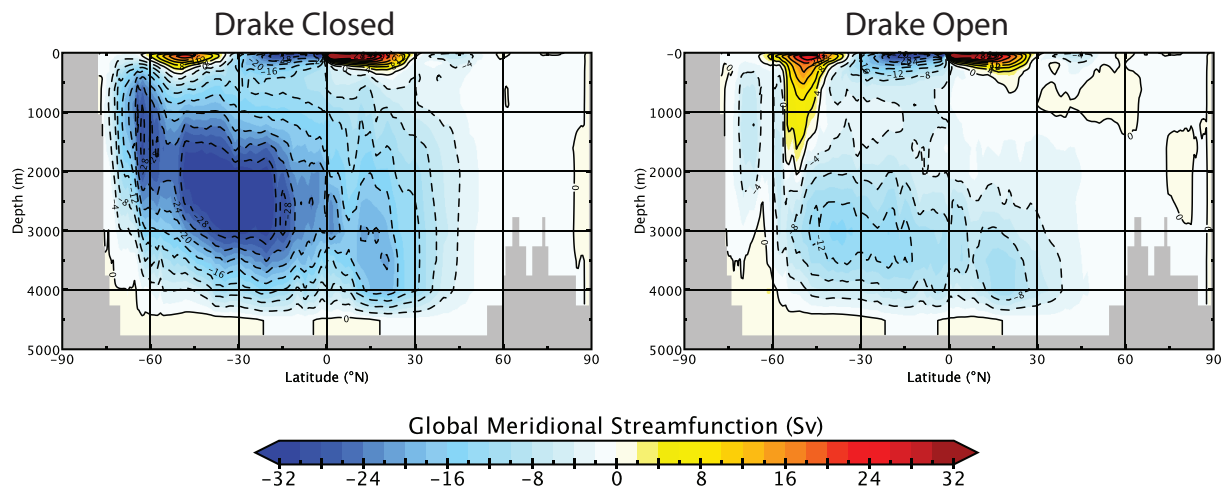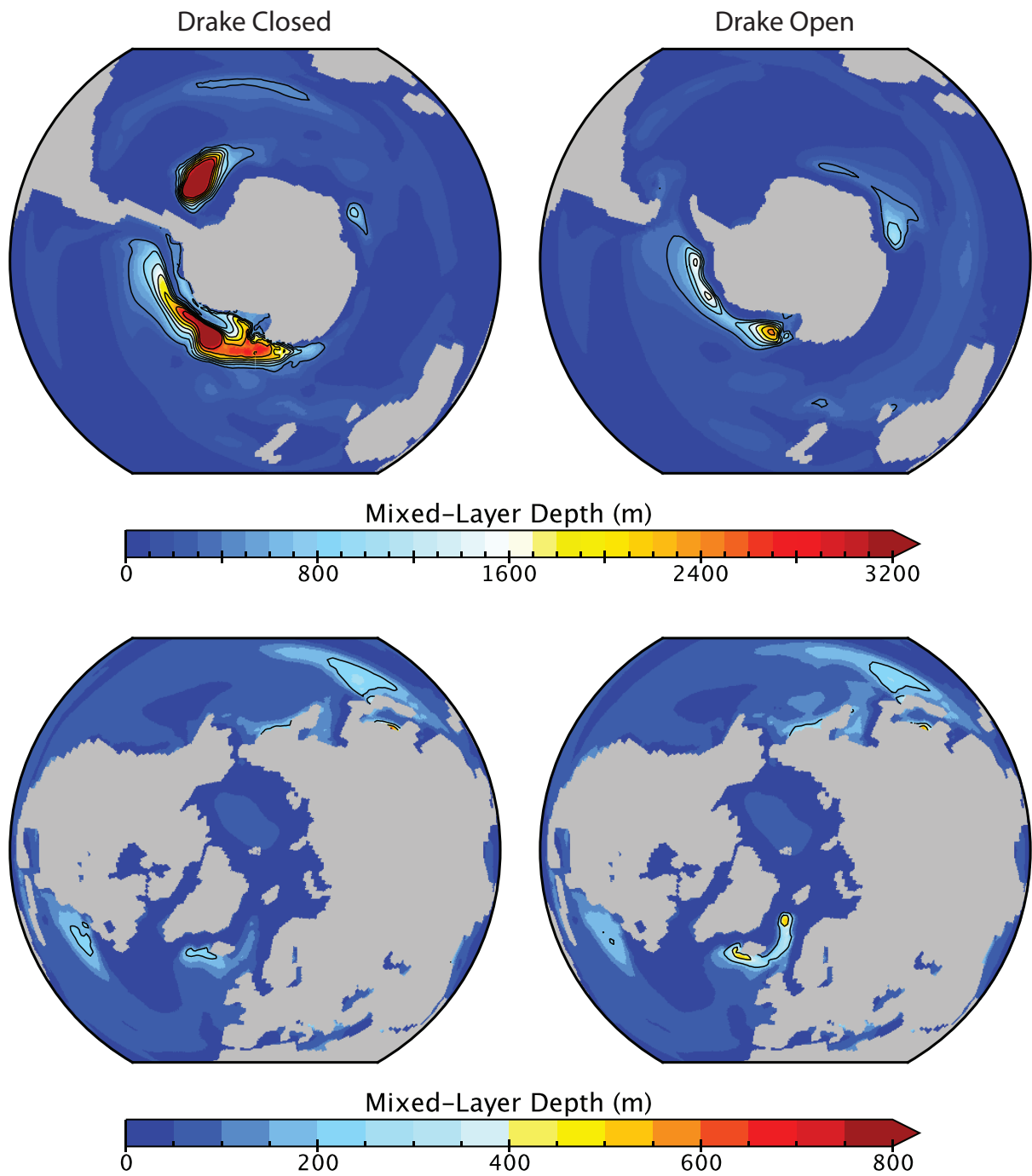
Figure 6.

873

874

875

876

877

DO-DC Diatoms   DO-DC Nanophytoplankton

Primary Productivity Difference (gC/m2/yr)

−50 −40 −30 −20 −10 0 10 20 30 40 50
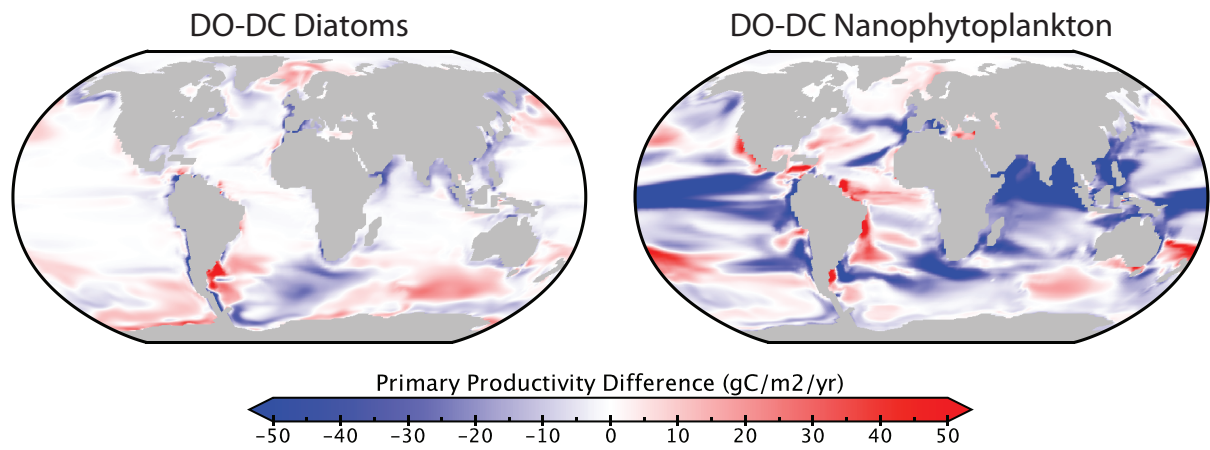
Figure 7.

878

879

880

Supplementary Materials for

Meridional contrasts in productivity changes driven by the opening of Drake Passage

Jean-Baptiste Ladant[1,2,3*], Yannick Donnadieu[1,4], Laurent Bopp[2,3], Caroline H. Lear[5], Paul A. Wilson[6]

[1]Laboratoire des Sciences du Climat et de l'Environnement, LSCE-IPSL, CEA / CNRS / UVSQ, Université Paris-Saclay, Gif-sur-Yvette, France.

[2]Ecole Normale Supérieure, Département de Géosciences, Paris, France.

[3]LMD / IPSL, CNRS / ENS / Ecole Polytechnique / UPMC, Paris, France.

[4]Aix Marseille Université, CNRS, IRD, Coll. France, CEREGE, Aix-en-Provence, France.

[5]School of Earth and Ocean Sciences, Cardiff University, Cardiff, UK.

[6]Ocean and Earth Science, National Oceanography Centre Southampton, University of Southampton, Southampton, UK.

Contents of this file

Figure S1 to S5
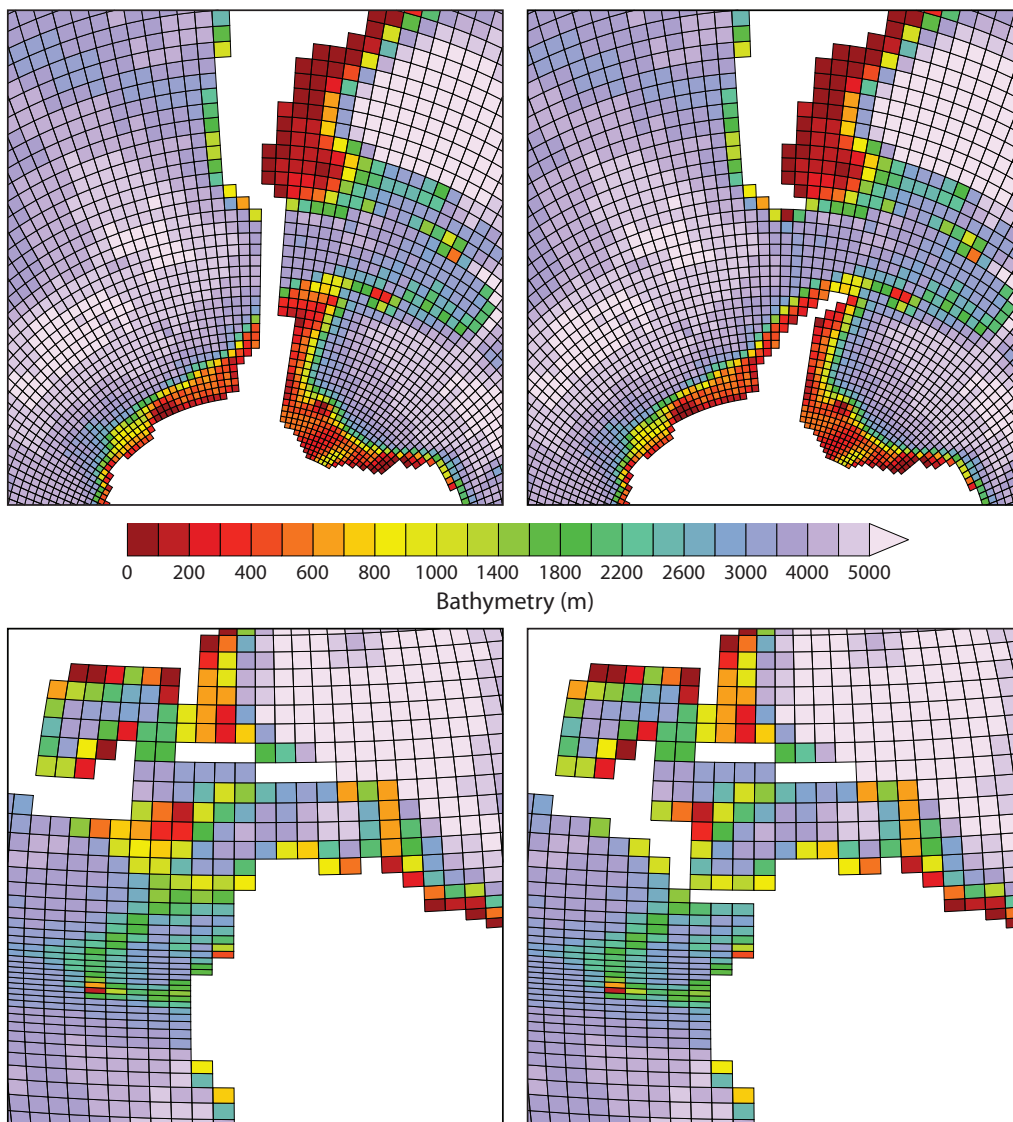
Figure S1. Drake Passage configurations in DC (upper left) and DO (upper right). The open geometry of the Panama Seaway (present both in DC and DO) is shown relative to present-day (bottom left and bottom right).
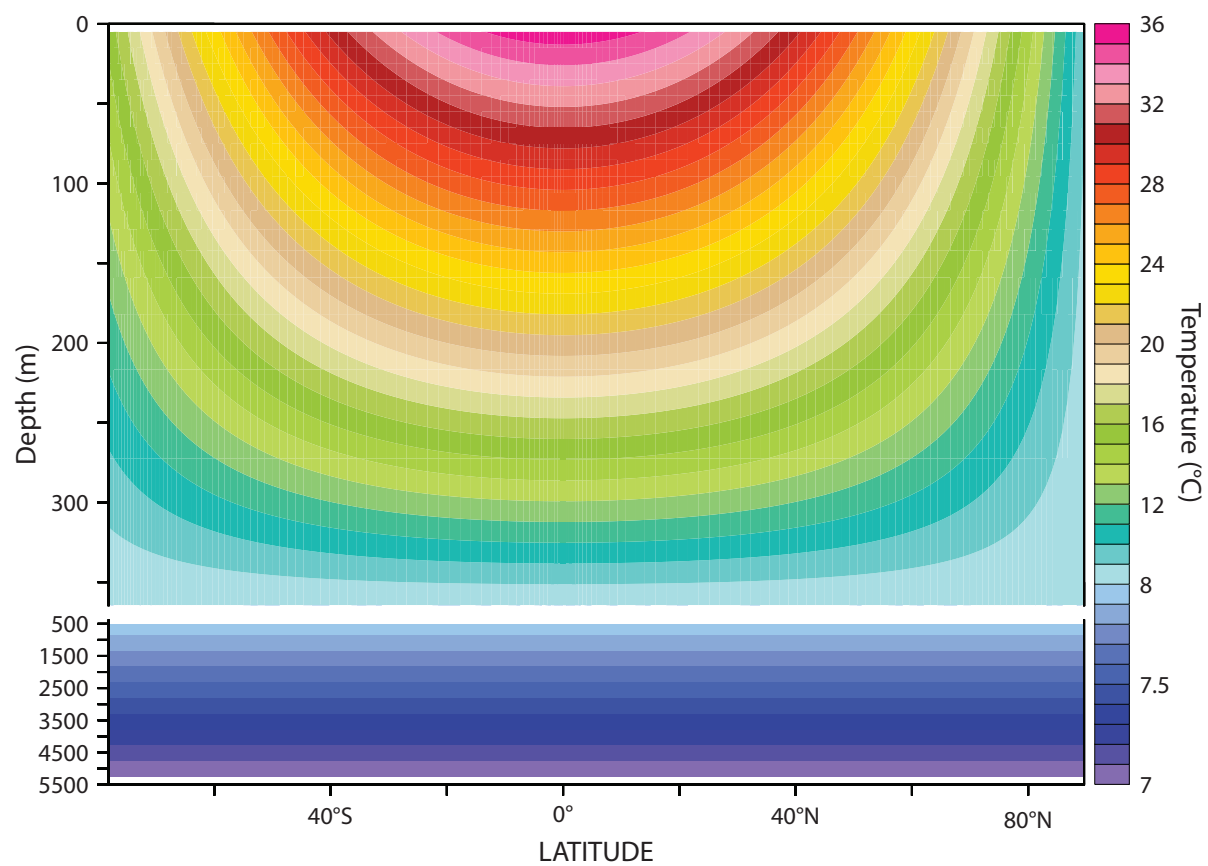
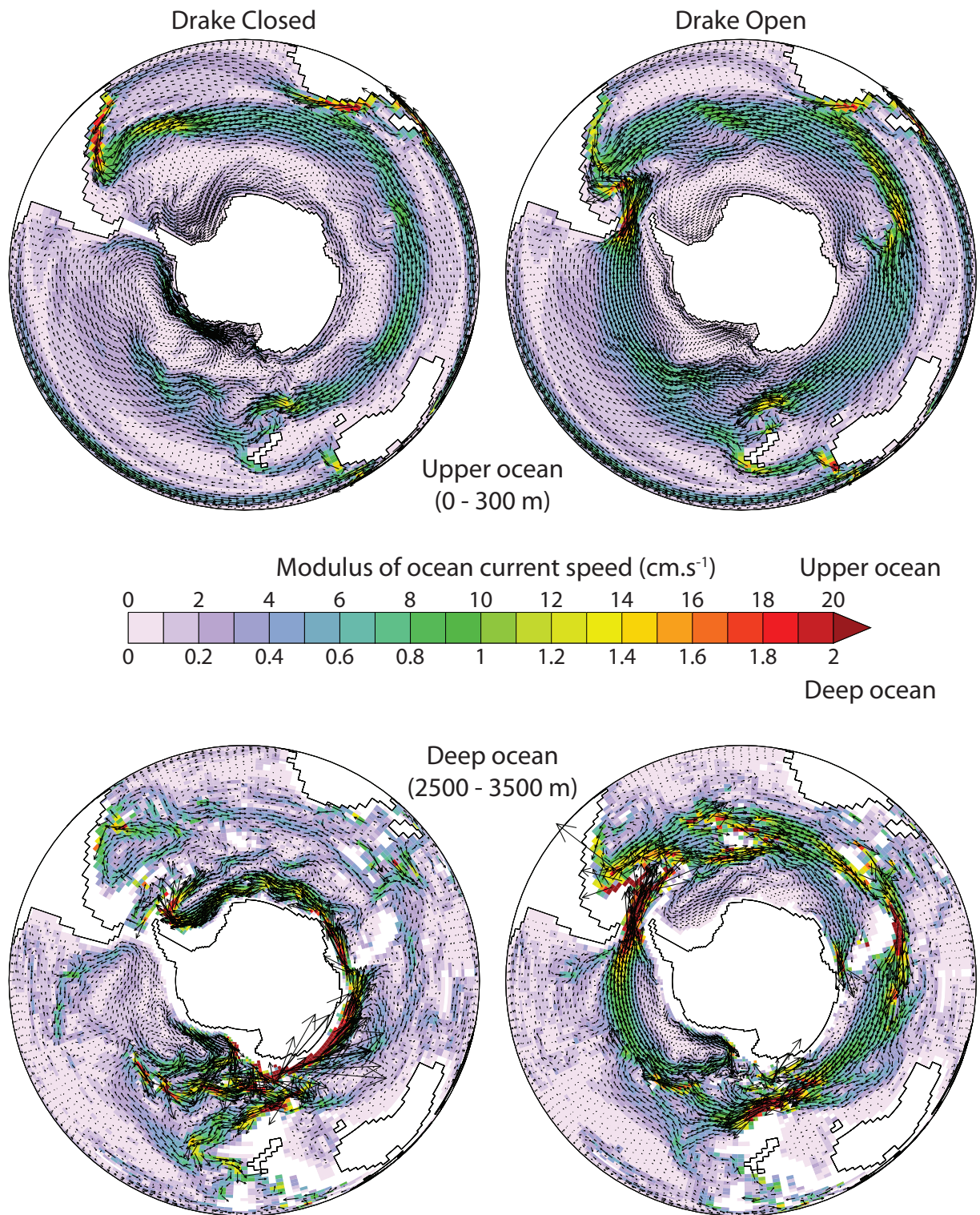**Figure S2.** Initial temperature state of the ocean.

Figure S3. Upper (0-300 m, top) and deep (2500-3500 m, bottom) oceanic current around Antarctica for DF (left) and DO (right) simulations.
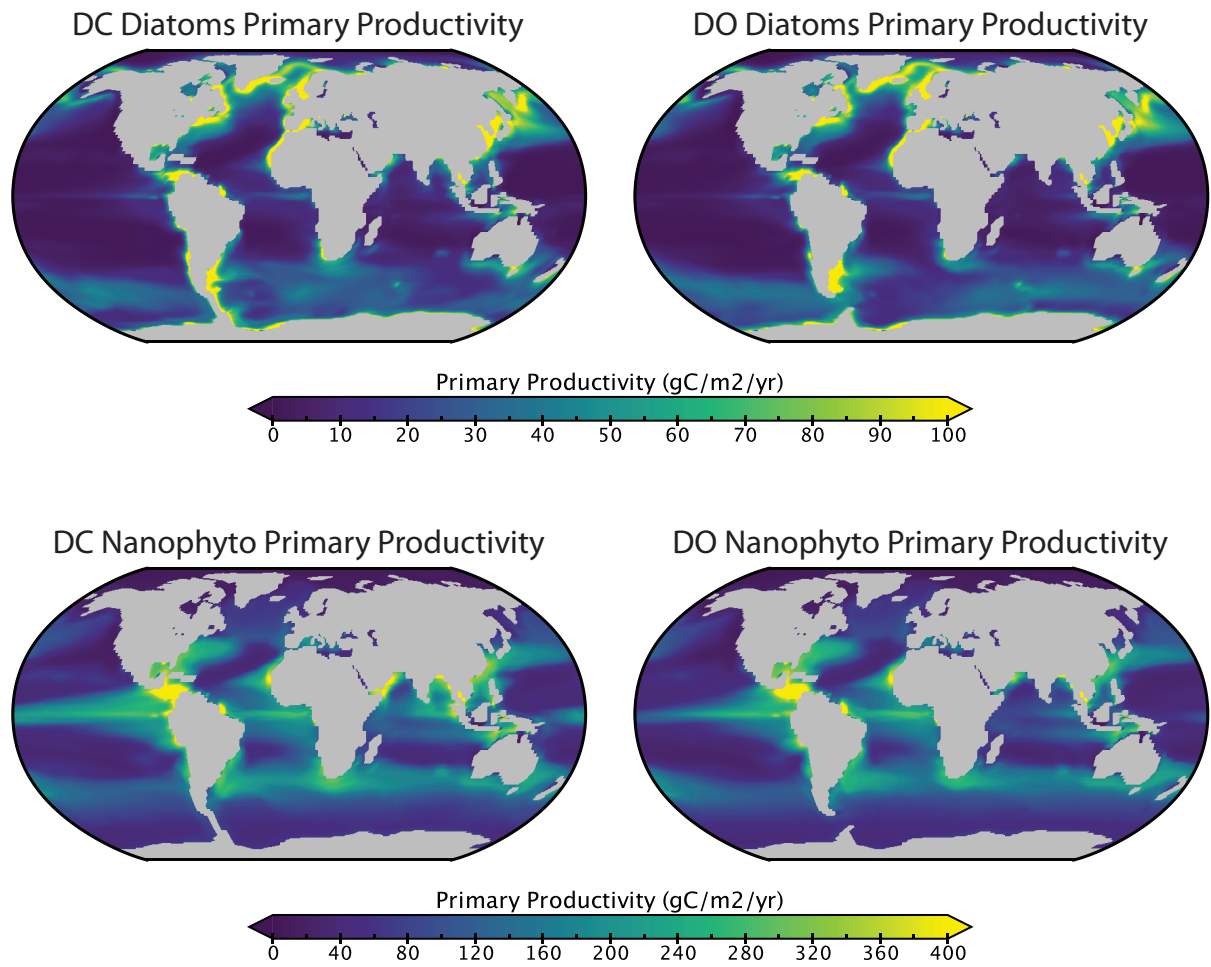
Figure S4. Mean annual diatoms (top) and nanophytoplankton (bottom) primary productivity for Drake Closed (left) and Drake Open (right) simulations.
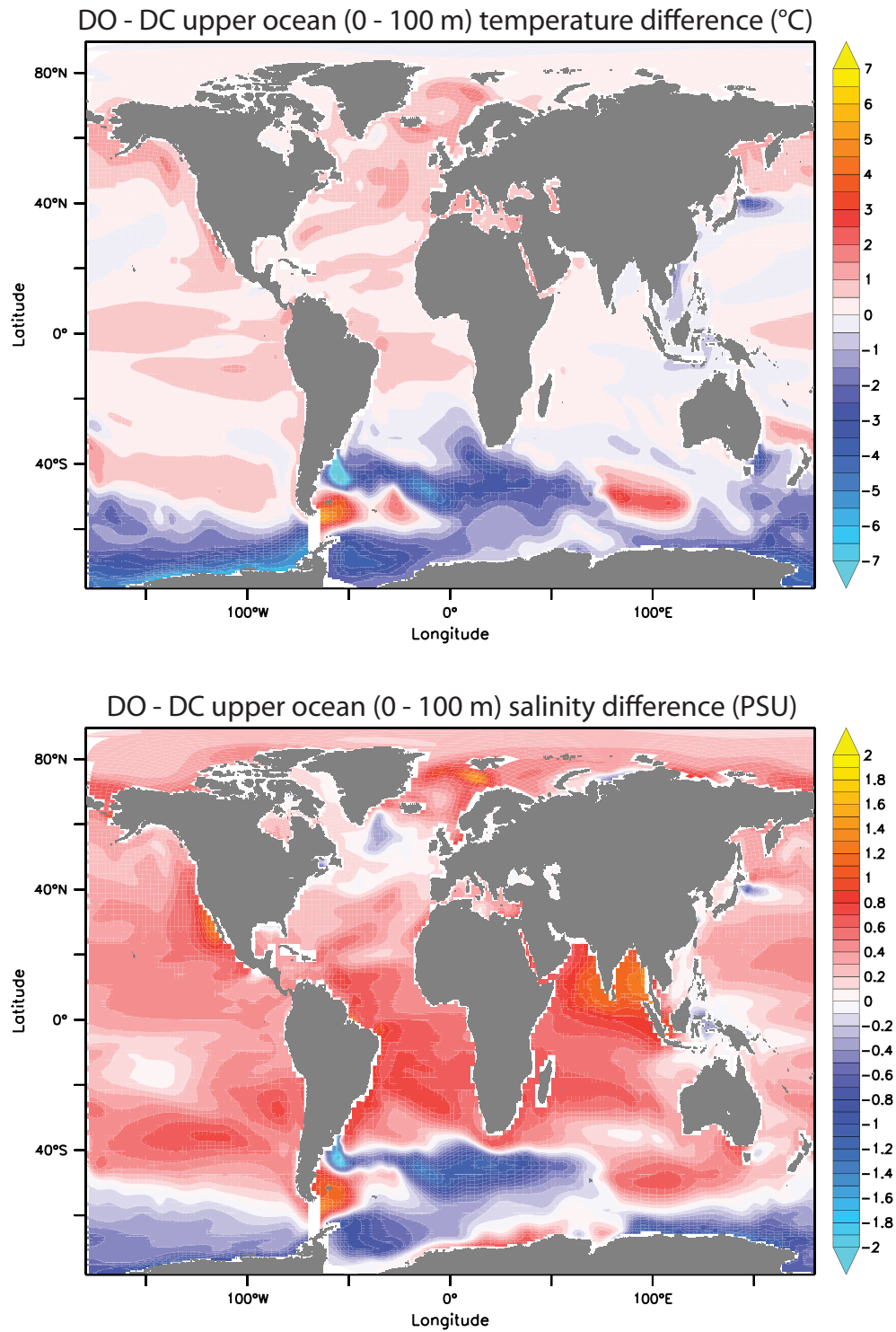
Figure S5. Surface ocean (0-100 m) temperature (top) and salinity (bottom) differences between DO and DF.